Journal of Biomolecular Structure and Dynamics

ISSN: (Print) (Online) Journal homepage: https://www.tandfonline.com/loi/tbsd20

Chemical library design, QSAR modeling and molecular dynamics simulations of naturally occurring coumarins as dual inhibitors of MAO-B and AChE

Yassir Boulaamane, Pallavi Kandpal, Anshuman Chandra, Mohammed Reda Britel & Amal Maurady

To cite this article: Yassir Boulaamane, Pallavi Kandpal, Anshuman Chandra, Mohammed Reda Britel & Amal Maurady (2023): Chemical library design, QSAR modeling and molecular dynamics simulations of naturally occurring coumarins as dual inhibitors of MAO-B and AChE, Journal of Biomolecular Structure and Dynamics, DOI: 10.1080/07391102.2023.2209650

To link to this article: https://doi.org/10.1080/07391102.2023.2209650

Published online: 18 May 2023.

JOURNAL OF BIOMOLECULAR STRUCTURE AND DYNAMICS
https://doi.org/10.1080/07391102.2023.2209650

Taylor & Francis
Taylor & Francis Group

Chemical library design, QSAR modeling and molecular dynamics simulations of naturally occurring coumarins as dual inhibitors of MAO-B and AChE

Yassir Boulaamane[a], Pallavi Kandpal[b], Anshuman Chandra[c], Mohammed Reda Britel[a] and Amal Maurady[a,d]

[a]Laboratory of Innovative Technologies, National School of Applied Sciences of Tangier, Abdelmalek Essaadi University, Tetouan, Morocco; [b]ProteinInsights, New Delhi, India; [c]ICMR-National Institute of Malaria Research, New Delhi, India; [d]Faculty of Sciences and Techniques of Tangier, Abdelmalek Essaadi University, Tetouan, Morocco

Communicated by Ramaswamy H. Sarma

ABSTRACT

Coumarins are a highly privileged scaffold in medicinal chemistry. It is present in many natural products and is reported to display various pharmacological properties. A large plethora of compounds based on the coumarin ring system have been synthesized and were found to possess biological activities such as anticonvulsant, antiviral, anti-inflammatory, antibacterial, antioxidant as well as neuroprotective properties. Despite the wide activity spectrum of coumarins, its naturally occurring derivatives are yet to be investigated in detail. In the current study, a chemical library was created to assemble all chemical information related to naturally occurring coumarins from the literature. Additionally, a multi-stage virtual screening combining QSAR modeling, molecular docking, and ADMET prediction was conducted against monoamine oxidase B and acetylcholinesterase, two relevant targets known for their neuroprotective properties and 'disease-modifying' potential in Parkinson's and Alzheimer's disease. Our findings revealed ten coumarin derivatives that may act as dual-target drugs against MAO-B and AChE. Two coumarin candidates were selected from the molecular docking study: CDB0738 and CDB0046 displayed favorable interactions for both proteins as well as suitable ADMET profiles. The stability of the selected coumarins was assessed through 100 ns molecular dynamics simulations which revealed promising stability through key molecular interactions for CDB0738 to act as dual inhibitor of MAO-B and AChE. However, experimental studies are necessary to evaluate the bioactivity of the proposed candidate. The current results may generate an increasing interest in bioprospecting naturally occurring coumarins as potential candidates against relevant macromolecular targets by encouraging virtual screening studies against our chemical library.

ARTICLE HISTORY
Received 19 February 2023
Accepted 5 April 2023

KEYWORDS
Coumarin; monoamine oxidase B; acetylcholinesterase; molecular docking; ADMET prediction; molecular dynamics simulations; QSAR modeling

1. Introduction

Neurodegenerative disorders such as Alzheimer's and Parkinson's disease remains the most frequent neurological diseases in the world (Barnham et al., 2004). Neurodegenerative diseases are characterized by the progressive loss of neuronal cells in the brain because of different factors contributing to its progression such as the deposition of amyloid fibrils, oxidative stress, mitochondrial dysfunction, and metal accumulation (Dugger & Dickson, 2017). Parkinson's disease (PD) is the second most frequent neurological disorder in the world that is described by the loss of dopaminergic neurons in the midbrain causing striatal dopamine deficiency (Poewe et al., 2017). It is estimated to affect six million people worldwide with an increasing prevalence expected to reach 2- to 3-fold by 2030 (Lee & Gilbert, 2016; Poewe & Mahlknecht, 2020). The most frequent motor symptoms are dyskinesia, shaking, and difficulty moving (Xia & Mao, 2012). Other non-motor symptoms may appear earlier such as depression, insomnia, and constipation (National Institute for Clinical Excellence, 2006). There is accumulating evidence indicating that oxidative damage and mitochondrial imbalance contribute to the cascade of events leading to the degeneration of the dopaminergic neurons (Dias et al., 2013). Thus, there is an increasing need for novel 'disease-modifying' therapies (Kalia et al., 2015). Current therapeutic strategies for PD treatment include L-DOPA therapy which remains the gold standard for controlling PD motor symptoms, other dopaminergic treatments include dopamine agonists, monoamine oxidase B (MAO-B) inhibitors and catechol-O-methyl transferase (COMT) inhibitors (Kaakkola, 2010; Lang & Marras, 2014). Non-dopaminergic treatments have also been proven to be effective for alleviating PD symptoms and slowing down neuronal damage such as adenosine A_{2A} receptor and N-methyl-D-aspartate (NMDA) receptor antagonists (Bara-Jimenez et al., 2003; Bibbiani et al., 2003). While acetylcholinesterase (AChE) inhibitors are mainly used to treat Alzheimer's disease, a clinical study has shown that AChE inhibitors may be efficacious for improving cognitive impairment and dementia in PD patients (Van Laar et al., 2011). Another recent meta-analysis included randomized controlled trials to investigate the effects of AChE inhibitors on PD's major symptoms, it was found that rivastigmine was effective for PD dementia (Chen et al., 2021). There's a great

CONTACT Amal Maurady amal.maurady.ma@gmail.com; Anshuman Chandra anshuman@nimr.org.in

deal of literature outlining the dual-activity of coumarin derivatives against MAO-B and AChE. Brühlmann et al. (2001) conducted an experimental study of a set of 17 coumarins with known inhibition against MAO enzymes against AChE, all the compounds inhibited AChE with values in the micromolar range ($3-100\,\mu M$) (Brühlmann et al., 2001). Another study reported the structural requirements of coumarins as dual inhibitors of MAO-B and AChE through molecular docking and structure-activity relationship analysis (Yusufzai et al., 2018). More recently, Ekström et al. (2022) synthetized a series of coumarins against MAO-B and AChE, the most potent compounds were bearing the N-methylbenzylamine moiety at position C7 and the N-benzylpiperidine moiety that is found in Donepezil, a reference AChE inhibitor that is prescribed to AD patients (Ekström et al., 2022).

Structural analysis of the crystallographic structure of MAO-B (PDB ID: 2V61) revealed that the latter is a dimer formed by a globular domain attached to the membrane through a C-terminal helix (Binda et al., 2007). The substrate fixing domain, located near the FAD cofactor binding domain, contains the active site of the enzyme. This active site is comprised of two cavities: an entrance cavity covered by the residues Pro-102, Pro-104, Leu164, Phe-168, Leu-171, and Ile-198, and a substrate cavity formed by Tyr-60, Cys-172, Tyr-188, Gln-206, Phe-343, Tyr-398, and Tyr-435 (Boulaamane et al., 2023). The residues Ile-199 and Tyr-326 act as 'gating' residues for the substrate cavity, playing a crucial role in determining substrate and inhibitor specificity for MAO-B (Milczek et al., 2011).

Meanwhile, the analysis of AChE crystal structure (PDB ID: 4EY7) revealed the presence of a dimer like MAO-B. The binding cavity is divided into the peripheral anionic site (PAS) formed by the residues: Trp-286, Tyr-337 and Phe-338; and the catalytic anionic site (CAS) which consists of the residues: Trp-86, Glu-202, Tyr-337 and Phe-338 (Pourshojaei et al., 2019). A study conducted with single and multiple site-specific mutants of mouse AChE revealed three distinct regions that confer selectivity for AChE inhibitors over butyrylcholinesterase (BChE). The first domain is defined by the acyl pocket dimensions, where the side chains of Phe-295 and Phe-297 primarily outline the acyl pocket dimensions. By replacing these phenylalanine side chains with the aliphatic residues found in BChE, the enzyme can catalyze larger substrates and accommodate selective BChE inhibitors. The second domain is found near the lip of the active center gorge defined by two tyrosines, Tyr-72 and Tyr-124, and by Trp-286. This region is crucial for the selectivity of bisquaternary inhibitors, such as BW284C51. The third domain is responsible for choline binding and defined by Tyr-337 [23]. The 3D structures of MAO-B and AChE along with their respective active sites are shown in Figure 1.

Despite the accumulating studies reporting the multi-target potential of synthetic drugs, the use of natural products against multiple therapeutic targets is yet to be investigated in detail (Lu et al., 2012). Numerous studies have reported the potency of natural products from medicinal plants, fruits, and vegetables to act as antiparkinsonian agents such as alkaloids, glycosides, flavonoids, caffeine, xanthones, catechins and coumarins which demonstrated neuroprotective properties associated with strong antioxidant and monoamine oxidase inhibitory activity (Carradori et al., 2014; Khanam et al., 2021; Singla et al., 2021).

Coumarins are phenolic compounds formed by fused benzene and α-pyrone rings (Garrard, 2014). Benzopyrones such as coumarins and flavonoids are present in many vegetables, fruit, seeds, nuts, coffee, tea, and wine (Lacy & O'Kennedy, 2004). Thus, dietary exposure to benzopyrones is considerable, which explains why extensive research into their pharmacological and therapeutic properties is underway over many years (Venugopala et al., 2013). A wide variety of coumarin derivatives have shown anticonvulsant, antiviral, anti-inflammatory, antibacterial, antioxidant and monoamine oxidase inhibitory activities (Stefanachi et al., 2018).

The growing volume of biomedical data in chemistry and biology requires development of new methods and approaches for their analysis (Tetko & Engkvist, 2020). *In silico* and data-driven approaches are much more time and cost effective compared to traditional experimental approaches (Zhao et al., 2020). They can rapidly screen large chemical libraries to identify promising leads (Pasrija et al., 2022). In fact, chemical libraries are essential databases for virtual drug screening. They consist of vast collections of chemical compounds with diverse structures and properties, allowing scientists to explore a wide range of potential drug candidates (Fukunishi & Lintuluoto, 2010). Furthermore, *in silico* methods allow for the generation of targeted libraries that focus on specific biological targets, chemical classes, or geographical regions. An illustrative example is the Benzylisoquinoline Alkaloids database (BIAdb), which encompasses over 800 plant-derived compounds of this chemical class enabling users to explore and obtain comprehensive information on these compounds (Singla et al., 2010).

Herein, we aimed to construct a chemical library of all available naturally occurring coumarins with their natural sources from which they were isolated to allow users to identify potential lead compounds and their source prior to their synthesis through high-throughput virtual screening. Furthermore, the chemical library was subject to a multi-stage virtual screening using quantitative structure-activity relationships (QSAR) models, molecular docking and ADMET evaluation to explore the potency of natural coumarins to act as dual inhibitors against MAO-B and AChE. Finally, the lead compounds were subject to 100 ns molecular dynamics simulations to further assess their stability over time.

2. Materials and methods

2.1. Data collection and chemical library design

PubMed search engine (https://pubmed.ncbi.nlm.nih.gov/) was employed to retrieve the available literature reporting the chemical data on coumarin containing compounds identified from natural sources using 'natural coumarins' as a search query. Our search revealed three book sections and one review article published in Progress in the Chemistry of Organic Natural Products in 1952, 2002, and 2017 and Journal of Pharmaceutical Sciences in 1964 respectively

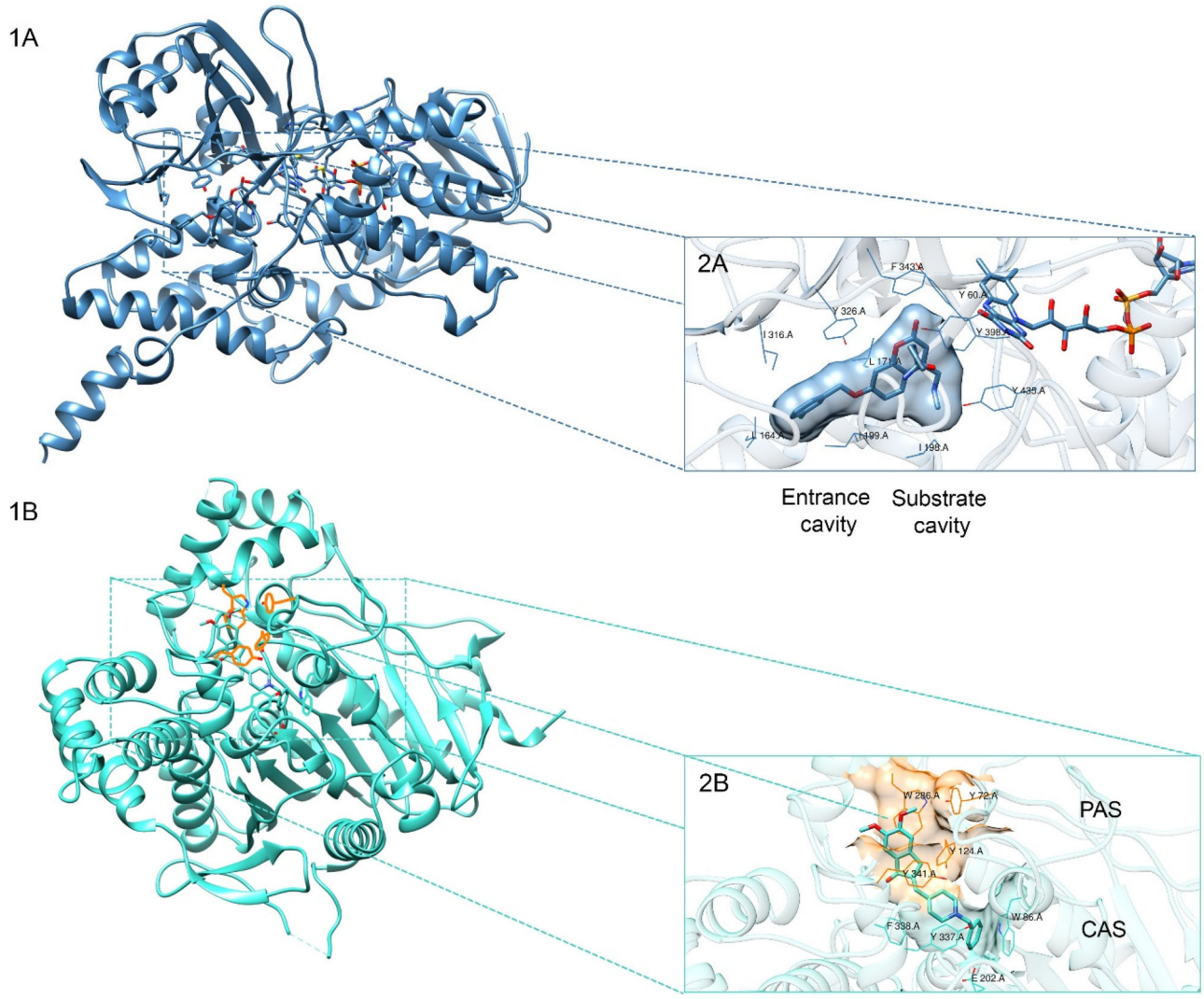

Figure 1. (1A) Crystal structure of MAO-B (PDB ID: 2V61) in complex with 7-(3- chlorobenzyloxy)-4-(methylamino)methyl-coumarin. (2A) Active site residues of MAO-B. (1B) Crystal structure of AChE (PDB ID: 4EY7) in complex with Donepezil. (2B) Active residues of the peripheral anionic site (PAS) and the catalytic anionic site (CAS) of AChE.

(Dean, 1952; Murray, 2002; Sarker & Nahar, 2017; Soine, 1964). The first step consisted of extracting the compound's names, chemical class, and natural sources. Subsequently, we searched the PubChem database to retrieve the PubChem IDs and chemical structures of all the compounds in SMILES format. OSIRIS DataWarrior software was used to generate unique chemical identifiers InChI Keys for all the molecules (Sander et al., 2015). Duplicate compounds were removed resulting in 905 unique natural coumarins. Furthermore, physicochemical properties such as lipophilicity, molecular weight, water solubility, number of hydrogen bond donors/acceptors, rotatable bonds, and polar surface area were computed as shown in Figure 2. All chemical information of the compounds can be found in CoumarinDB (https://yboulaamane.github.io/CoumarinDB/).

2.2. QSAR modeling

From ChEMBL database (https://www.ebi.ac.uk/chembl/), we retrieved two datasets containing chemical structures that were classified according to their calculated activity, including 5066 MAO-B inhibitors and 8846 AChE inhibitors with reported half maximal inhibitory concentration (IC_{50}) values (Mendez et al., 2019). The datasets were manually curated, duplicate compounds were removed when multiple bioactivity values were reported for a given compound by calculating the mean value of the 'Standard Value' column in the pandas DataFrame grouped by the 'Molecule ChEMBL ID' column. The resulting mean values are added to a new column in the DataFrame called 'mean_value'. Thereafter, the DataFrame.drop_duplicates function included in the Pandas library (McKinney, 2011) was used to identify and remove duplicate rows in the dataset based on the values in the 'Molecule ChEMBL ID' column to keep only one occurrence.

Logarithmic transformation was applied to all the activity values to better determine the potency of the compounds (Burggraaff et al., 2020; Tarasova et al., 2015). The workflow of QSAR modeling is shown in Figure 3.

The datasets were then converted to SMILES format, RDKit cheminformatics software was used to generate molecular descriptors using Morgan fingerprints (Ding et al., 2021; Landrum, 2013). The IC_{50} values were converted to

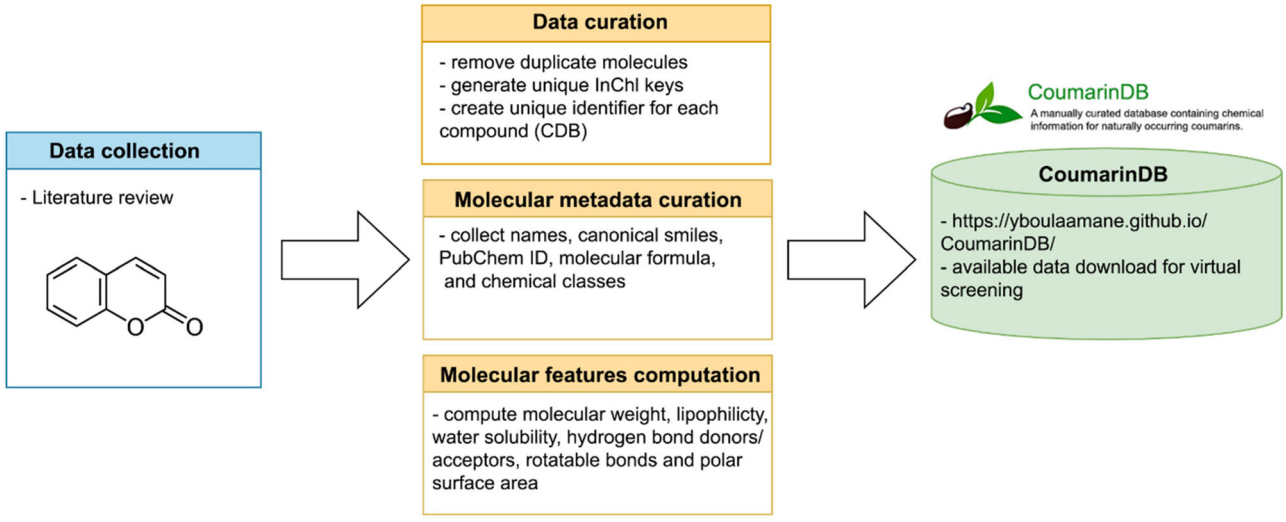

Figure 2. Chemical library construction and curation of CoumarinDB.

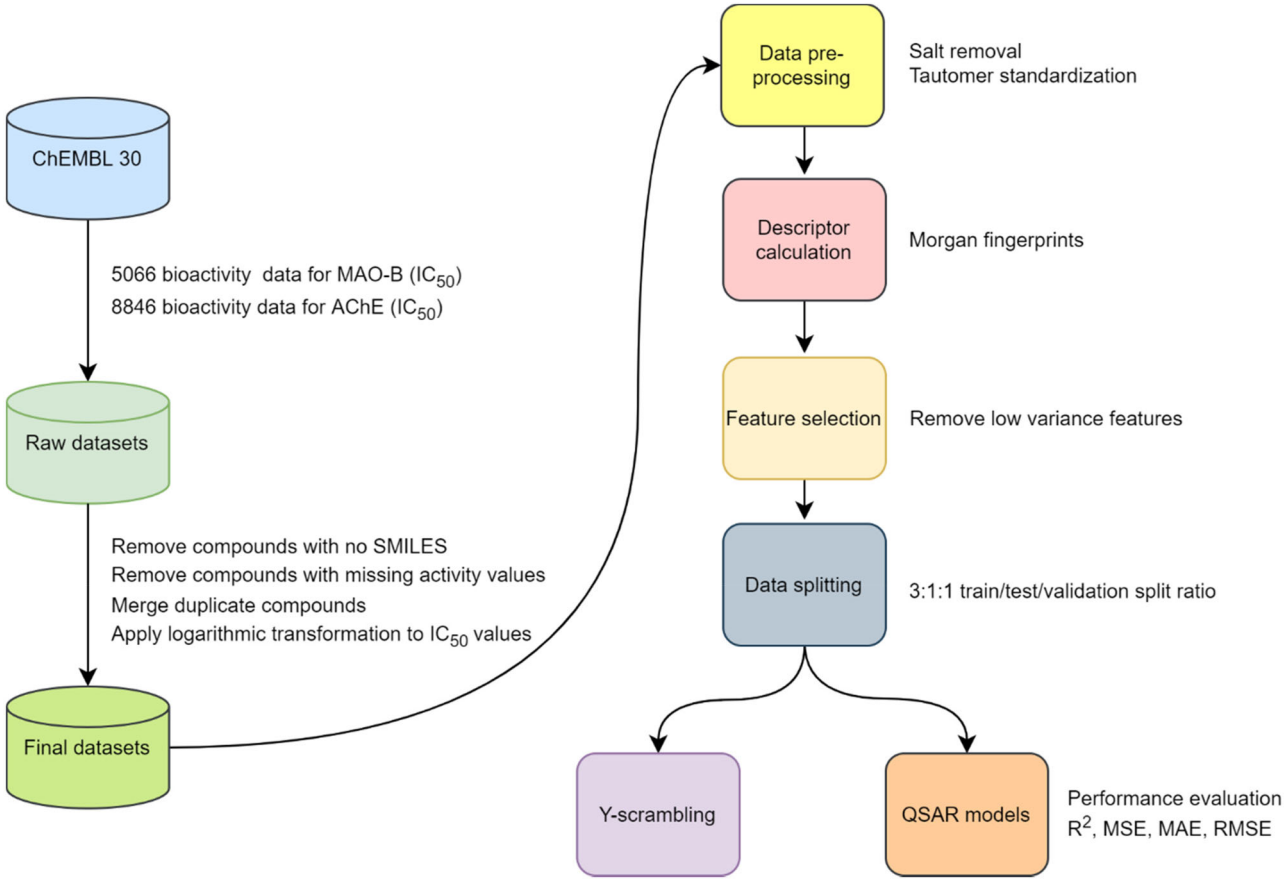

Figure 3. QSAR workflow for modelling the bioactivity prediction of MAO-B and AChE.

Table 1. Distribution of the molecules in the training, testing and validation dataset.

Dataset	Train set	Test set	Validation set	Total dataset
Number of Molecules in MAO-B dataset	2526	842	843	4211
Number of Molecules in AChE dataset	2618	873	873	4363

pIC_{50} for ease of handling. The dataset was split into a 3:1:1 ratio of training, testing and validation sets. The number of molecules in each of them is listed in Table 1.

Machine learning algorithms like multiple linear regression (MLR), random forest (RF), decision trees (DT), support vector regression (SVR), AdaBoost and extreme gradient boosting (XGB) were used for building the model (Wu et al., 2021). These models were built with all the hyperparameters set to default and were assessed using validation metrics such as the coefficient of determination (R^2), mean squared error

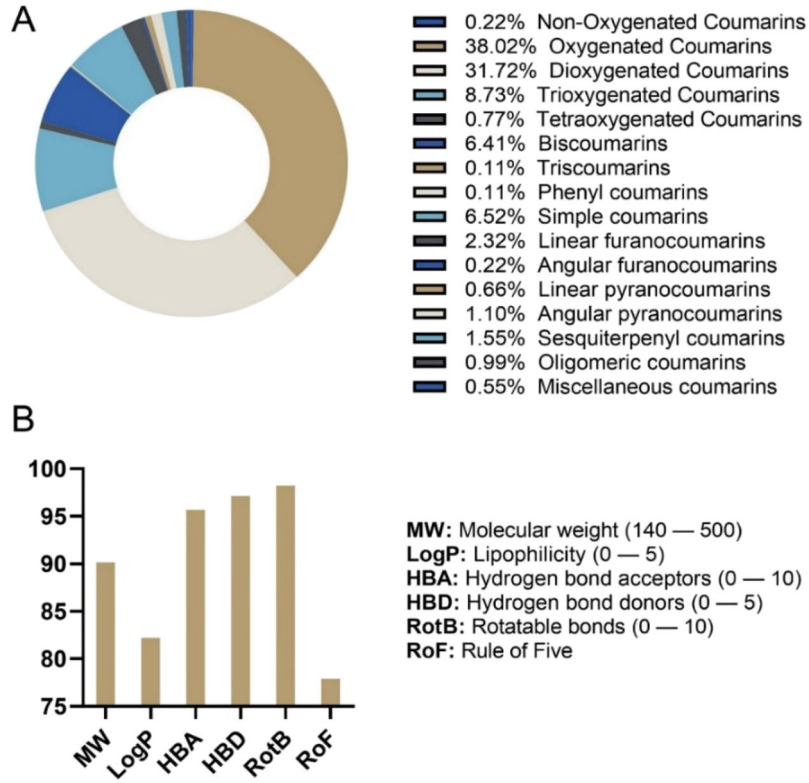

Figure 4. (A) Chemical class distribution of naturally occurring coumarins. (B) Percentage of compounds in the recommended range for each physicochemical parameter of the rule of five.

(MSE), mean absolute error (MAE) and root mean squared error (RMSE). The QSAR workflow is illustrated represented in Figure 3.

2.3. Preparation of ligand structures

The designed library of coumarins was found to contain mostly oxygenated and deoxygenated coumarins as shown in Figure 4A. Primary filtration was conducted based on Lipinski's rule of five. 706 out of 905 (78%) molecules were retained for the present study as drug-like compounds (Figure 4B). OSIRIS DataWarrior cheminformatics program was used to generate an SDF file for all the ligands (Sander et al., 2015). Thereafter, the OpenBabel toolbox was used to split the compounds and optimize the chemical structures using MMFF94 force field (Halgren, 1996; O'Boyle et al., 2011). Partial charges and atom types were computed for the molecular docking study.

2.4. Molecular docking

Crystallographic structure of MAO-B (PDB ID: 2V61, resolution = 1.7 Å) in complex with a coumarin derivative, 7-(3- chloro-benzyloxy)-4-(methylamino) methyl-coumarin (C18) was retrieved from the RCSB PDB (https://www.rcsb.org/) (Binda et al., 2007). Alternatively, crystal structure of AChE (PDB ID: 4EY7, resolution = 2.3 Å) in complex with Donepezil (E20) was selected for the molecular docking (Cheung et al., 2012). Native ligands and crystal water molecules were removed to make computations easier and clear the binding pocket of possible water molecules that would distort the pose search. Chain B was removed from both protein dimers and only one chain was kept for the molecular docking along with the FAD cofactor in MAO-B as it plays an important role in the proper functioning of the enzyme in catalyzing the deamination of monoamines (Edmondson & Newton-Vinson, 2001). Residues with missing atoms were fixed using the CHARMM-GUI web server (Jo et al., 2008). Polar hydrogen and Kollman charges were added using AutoDockTools (Huey & Morris, 2008). Finally, the native ligands were used to define the grid box parameters to cover the entire binding sites residues. The grid box was generated largely enough to fit all the active site residues of MAO-B and AChE ($24 \times 24 \times 24$ Å) in x, y and z directions, respectively. The grid box was placed in a way to cover both cavities in the selected targets and to allow larger molecules to dock properly ($51.2 \times 155.5 \times 28.7$ Å and $-14.1 \times -43.8 \times 27.7$ Å for MAO-B and AChE respectively). Molecular docking was performed using AutoDock Vina with an exhaustivness = 8 and num_modes = 10 (representing 10 conformations) (Trott & Olson, 2010).

2.5. ADME/tox prediction

Forty percent of drug candidates fail in clinical trials due to unfavorable pharmacokinetic properties (Lin et al., 2003). *In silico* open access tools for predicting Absorption, Distribution, Metabolism, Excretion and Toxicity (ADMET) parameters have emerged as a cost-efficient approach in the early phases of drug development (Gola et al., 2006). The pharmacokinetics and toxicity parameters for the selected

Table 2. The validation metrics of the algorithms used at default hyperparameters.

	MAO-B Dataset				AChE Dataset			
Algorithm	R^2	MSE	MAE	RMSE	R^2	MSE	MAE	RMSE
MLR	0.19	2.96	4.68	4.54	−0.24	10.3	2.13	3.21
RF	0.72	0.65	0.58	0.81	0.67	1.11	0.70	1.05
DT	0.30	1.14	0.71	1.07	0.52	1.58	0.77	1.26
SVR	0.59	0.68	0.59	0.82	0.70	1.01	0.67	1.00
AdaBoost	0.20	1.32	0.95	1.15	0.34	2.19	1.27	1.48
XGB	0.60	0.65	0.58	0.81	0.69	1.01	0.69	1.01

coumarins such as water solubility, intestinal absorption, blood-brain barrier permeability, drug-drug interactions, Ames toxicity and hepatotoxicity were computed using pkCSM online calculation tool (http://biosig.unimelb.edu.au/pkcsm/) (Pires et al., 2015).

2.6. Molecular dynamics workflow

Two compounds which demonstrated great affinity towards MAO-B and AChE as well as great pharmacokinetics properties were selected from the molecular docking study to perform MD simulations to study the stability of the protein-ligand complexes over time. Desmond module of Schrödinger's suite (2020-3) was used to run 100 ns MD simulation (Bowers et al., 2006). The water-soaked solvated system was created in Desmond using the System Builder panel. OPLS2005 force field was selected, and Single Point Charge (SPC) was used as a solvent model with a 10 Å orthorhombic box for both proteins (Shivakumar et al., 2010). The system was neutralized by randomly adding enough counter-ions (Na^+ and Cl^-) and isosmotic state was maintained by adding 0.15 M NaCl. The solvated model system was subjected to energy minimization using OPLS2005 force field parameters as the default protocol associated with Desmond (Boulaamane et al., 2023). Then, the system was equilibrated throughout the simulation time *via* NPT ensemble at a constant 300 K temperature and 1 atm pressure using the Nose-Hoover thermostat algorithm and Martyna-Tobias-Klein barostat algorithm, respectively (Melchionna et al., 1993; Möller et al., 1992). A total of 100 ns simulations were carried out, during which 1000 frames were recorded. Finally, MD simulation trajectory was analyzed using the Simulation Interaction Diagram (SID) tool (Katari et al., 2016).

3. Results and discussion

3.1. QSAR models validation

The performance of the generated machine learning models is presented in Table 2. The MLR algorithm performed the worst of all on the MAO-B dataset with a very low value (0.19) and on the AChE dataset with a negative R^2 and a corresponding high error rate. AdaBoost performed better than MLR on both the datasets, however R^2 was still below 0.5, and MSE value was high. A better performance was observed by the SVR, XGB and RF algorithm with an R^2 value of 0.59, 0.60, and 0.61 respectively, on the MAO-B dataset. Moreover, a better metric was obtained using these algorithms on the AChE dataset. However, the best model amongst all was RF with an R^2 value of 0.72 and MSE of 0.65, for the MAO-B dataset and for the AChE dataset, it was SVR with an R^2 value of 0.70 and MSE of 1.01.

Table 3. The grid parameters of SVR algorithm used in GridSearchCV*.

Dataset	Hyperparameter	Values
MAO-B	n_estimators	200–2000, step = 10
	max_features	'auto,' 'sqrt'
	max_depth	10–110, step = 11
	min_sample_split	2, 5, 10
	min_sample_leaf	1, 2, 4
	bootstrap	'True,' 'False'
AChE	kernel	'linear,' 'rbf', 'sigmoid', 'poly'
	tolerance	1e-3, 1e-4, 1e-5, 1e-6
	C	1, 1.5, 2, 2.5, 3
	degree	1, 2, 3, 4, 5, 6
	gamma	'scale,' 'auto'

*The acronyms for the various parameters are as mentioned in the scikit-learn documentation.

Since the best of all the algorithms used was RF for the MAO-B dataset and SVR for the AChE dataset, the hyperparameters were set to be optimized using the GridSearchCV function in Scikit-Learn. The algorithm was extensively searched using the RepeatedKFold, where number of folds was set to 10 with 3 repeats and with parameters as presented in Table 3.

The best model of all the parameters for the SVR was found to be with kernel: rbf, C:3, tol: 1e-0.5, gamma: 'scale' and degree: 3. The model was improved and an r^2 value of 0.74 and MSE of 0.86 was obtained. For the MAO-B dataset, the best RF parameters were found to be at n_estimators = 800, min_samples_split = 5, min_samples_leaf = 1, max_features = 'sqrt', max_depth = 90, bootstrap = False. The model was found to show an r^2 value of 0.65 and MSE of 0.58. These models were also applied to the validation set (for their respective datasets). The evaluation metrics for the test and validation set are given in Table 4.

To ascertain that the evaluation metrics obtained were not obtained by-chance correlation, a y-scrambling was performed for five times, where the associated pIC_{50} values for the molecules in the training set were jumbled, the model was 'fit' using them and predicted for the test set. The goal was to check if the model performs worse, indicating that there is no chance correlation in the model. The results are presented in Table 5. All the 5 models generated performed poorly, with high error metrics and a negative correlation value, thereby indicating that the model used here is robust.

The models with the best hyperparameters of RF and SVR algorithm were applied to the dataset of the naturally occurring coumarins (having 706 molecules) to identify potential leads for biological evaluation. The top molecules are presented in Figure 5.

3.2. Molecular docking results

The molecular docking protocol implemented in AutoDock Vina was validated by redocking the crystal ligands of MAO-B and AChE against their respective binding sites (Mateev et al., 2022; Trott & Olson, 2010). Co-crystallized ligands were downloaded from PubChem database and prepared using

the same parameters for the tested ligands (Kim et al., 2019). The root-mean-square deviation (RMSD) was calculated by superposing both docked and native ligands, the latter was used as a reference. The results yielded values of 0.87 Å for MAO-B and 0.98 Å for AChE demonstrating a good accuracy of the docking program (Figure 6).

The top scoring, common molecules predicted by both the datasets were then docked into the active site of MAO-B and AChE using AutoDock Vina (Trott & Olson, 2010). The best conformations of the docked compounds were selected based on their binding affinity and their similarity to the co-crystallized ligands by means of superposition. Hydrogen bonds and nearby hydrophobic interactions were visualized using DS Visualizer (Biovia, 2017). Docking scores and hydrogen bonds of the best candidates along with the reference inhibitors are displayed in Table 6.

Molecular interactions analysis was conducted for the two highest-scoring candidates (Figures 7 and 8). CDB0738 revealed the presence of a hydrogen bond involving Gln-206 which is known to act as a hydrogen bond acceptor for most MAO-B inhibitors (Boulaamane et al., 2022). Another hydrogen bond was found to involve Tyr-435 of the aromatic cage. A π-π stacking interaction was observed between the pyrone ring of the coumarin scaffold and Tyr-326, a key aromatic residue, suggesting potential selectivity for MAO-B over MAO-A where this residue is replaced by the aliphatic amino acid, Ile-335. Meanwhile, CDB0046 formed a hydrogen bond with Pro-102, a rigid residue located at the extremity of the entrance cavity of the MAO-B binding pocket. This interaction may be attributed to the larger size of the compound, potentially conferring selectivity for MAO-B over MAO-A, as the latter has a smaller cavity and cannot accommodate bulkier compounds. An additional hydrogen bond was observed between CDB0046 and Cys-172, a residue located in the catalytic site of MAO-B. It's important to note that this residue is not conserved in both isoenzymes. In MAO-A, Cys-172 is replaced by Asn-171, and Cys-323 is in the opposite side of the binding pocket, further adding to the potential selectivity of the studied coumarin (Di Paolo et al., 2019).

On the other hand, CDB0738 formed a hydrogen bond with Glu-202 located in the choline binding site of AChE. This interaction plays an essential role in maintaining the critical hydrogen bond network required to support the catalytic triad of AChE (Wang et al., 2022). CDB0738 also exhibited two additional π-π stacking interactions involving the aromatic amino acids Trp-86 and Tyr-341 known for stabilizing AChE inhibitors (Ranjan et al., 2015). In contrast, CDB0046 formed four hydrogen bonds with Tyr-72, a residue known to be critical for the selectivity of bisquaternary inhibitors (Radic et al., 1993). The 3-hydroxy-3-(hydroxymethyl)-5-

Table 4. The evaluation metrics using the best model generated from hyperparameter tuning.

Dataset	Algorithm	R^2	MSE	MAE	RMSE
MAO-B	Test Set	0.78	0.58	0.56	0.76
	Validation Set	0.75	0.60	0.58	0.78
AChE	Test Set	0.74	0.86	0.62	0.93
	Validation Set	0.76	0.79	0.59	0.89

Table 5. The highest values obtained for r2 and MSE for the y-scrambled dataset.

Dataset	y-scrambled models	R^2	MSE	MAE	RMSE
MAO-B	Y_1	−0.25	2.05	1.15	1.43
(Using the RF with	Y_2	−0.19	1.97	1.11	1.40
best parameters)	Y_3	−0.16	1.91	1.11	1.38
	Y_4	−0.08	1.78	1.07	1.33
	Y_5	−0.15	1.90	1.10	1.38
AChE	Y_1	−0.14	3.76	1.62	1.94
(Using the SVR with	Y_2	−0.14	3.76	1.60	1.94
best parameters)	Y_3	−0.25	4.12	1.69	2.03
	Y_4	−0.19	3.94	1.62	1.98
	Y_5	−0.24	4.08	1.65	2.02

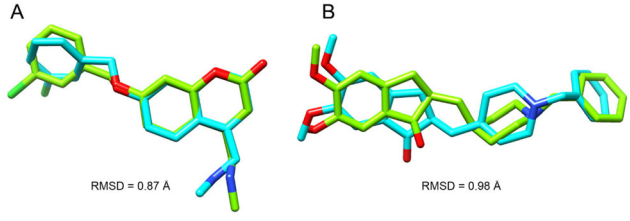

Figure 6. RMSD values and Superimposition of native co-crystallized (cyan color) and docked ligands (chartreuse color) for MAO-B (A) and AChE (B).

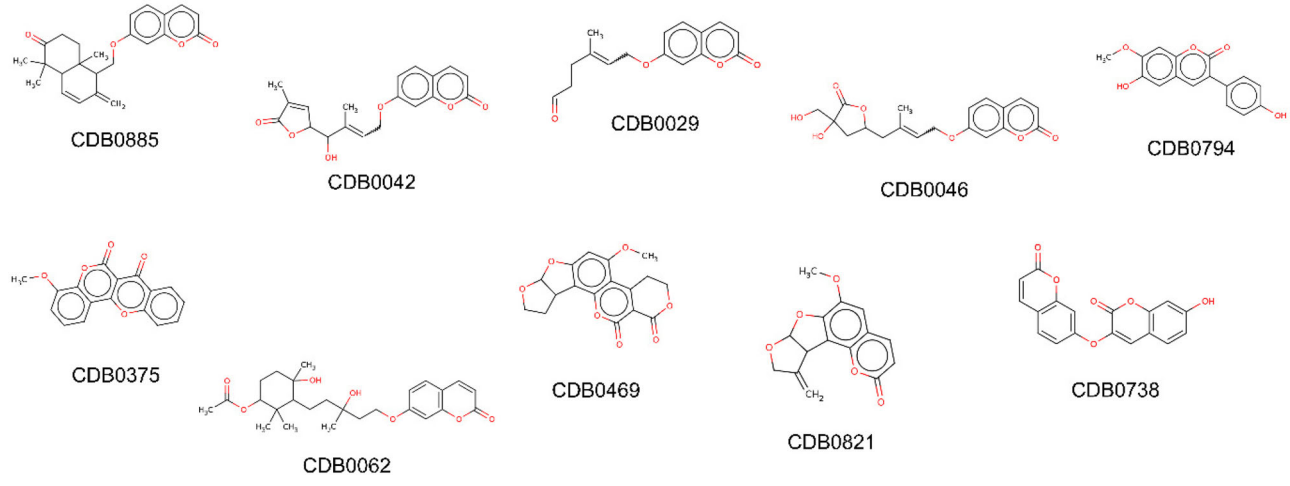

Figure 5. Top ranked molecules with predicted $pIC_{50} > 6$ by the RF and SVR models created using MAO-B and AChE respectively.

Table 6. Molecular docking results of the selected naturally occurring coumarins against MAO-B and AChE.

		Docking score (kcal/mol)		Hydrogen bonds		π-π interactions	
Compound	Natural source	MAO-B	AChE	MAO-B	AChE	MAO-B	AChE
C18[a]	—	−9.8	−10.5	Cys-172	Ser-125 His-447	Tyr-326 Tyr-398	Trp-286 Phe-338 Tyr-341
E20[b]	—	−7.9	−11.3	—	Phe-295	Phe-343	Trp-86 Tyr-341
CDB0738	*Edgeworthia chrysantha*	−12.7	−12.4	Gln-206 Tyr-435	Glu-202	Tyr-326 Tyr-398	Trp-86 Tyr-341
CDB0046	*Clausena excavata*	−9.7	−11.1	Pro-102 Cys-172	Tyr-72 Gly-121 Glu-202 Ser-203	Tyr-398 Tyr-435	Trp-286
CDB0042	*Clausena excavata*	−9.9	−10.9	Tyr-188 Ile-199	Tyr-72 Gly-121 Ser-203	Tyr-398	Trp-286
CDB0885	*Ferula narthex*	−7.5	−12.6	Tyr-435	Tyr-72	Tyr-398	Trp-286 Tyr-341
CDB0794	*Nicotiana tabacum*	−9.3	−10.3	Cys-172 Tyr-435	—	Tyr-326	Tyr-337 Tyr-341
CDB0029	*Aegle marmelos*	−9.3	−9.4	Tyr-435	—	Tyr-398	Tyr-341
CDB0375	*Polygala fruticosa*	−7.9	−10.2	—	—	Tyr-326 Tyr-398 Tyr-435	Trp-286 Tyr-337 Tyr-341
CDB0062	*Ferula polyantha*	−5.8	−10.8	—	Gly-121 Ser-203	Tyr-398 Tyr-435	Trp-286
CDB0469	*Aspergillus flavus*	−5.8	−10.5	—	Tyr-124 Tyr-133	Leu-171	Trp-86
CDB0821	*Micromelum minutum*	−5.5	−9.2	—	Tyr-124	Tyr-326 Tyr-398	Tyr-337

[a]7-(3- chlorobenzyloxy)-4-(methylamino)methyl-coumarin; [b]Donepezil.

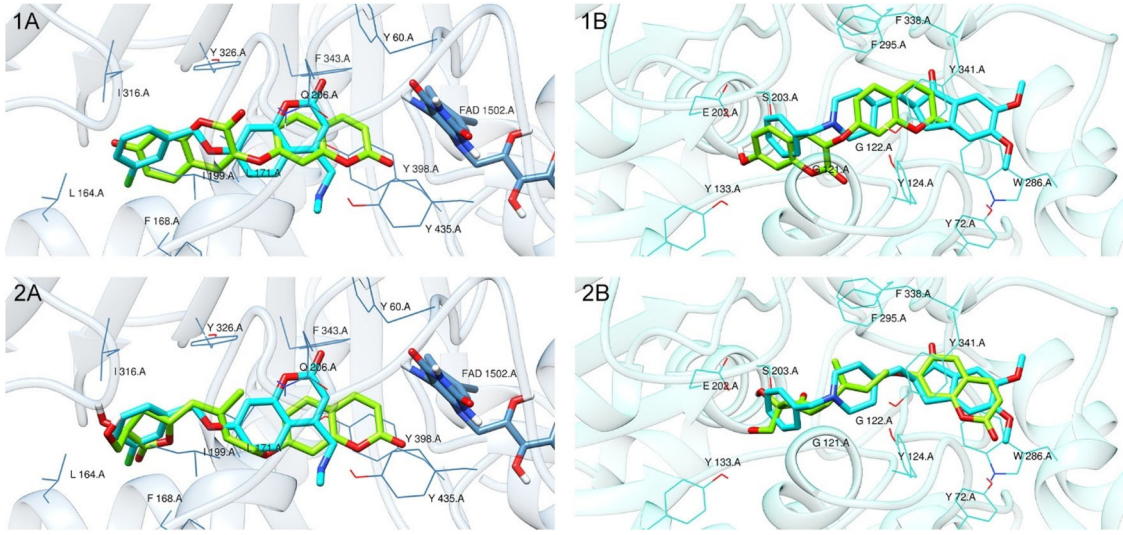

Figure 7. Docking conformations of the selected coumarin candidates (chartreuse color) superposed to reference ligands (cyan color). (1A) CDB0738-MAO-B complex; (2A) CDB0046-MAO-B complex; (1B) CDB0738-AChE complex; (2B) CDB0046-AChE complex.

methyloxolan-2-one moiety linked to the coumarin scaffold was responsible for the other observed hydrogen bonds involving Gly-121, Glu-202, and Ser-203. Moreover, the coumarin scaffold formed two π-π stacking interactions with Trp-286 located in the PAS of AChE. Trp-286 is thought to play a crucial role in the allosteric modulation of human AChE activity by binding to ligands at the entrance of the active site gorge. Mutations of Trp-286 have been shown to result in a significant decrease in binding affinity of PAS ligands, indicating its importance in the ligand recognition (Barak et al., 1994).

3.3. ADME/tox prediction results

ADME and toxicity prediction results for the selected coumarins are shown in Table 7. pkCSM predicted water solubility show that all the compounds have values ranging between −3.2 and −5.5 which are within the recommended range (–6.5 to 0.5) where 95% of similar values for known drugs fall inside (Ntie-Kang, 2013). Predicted intestinal absorption shows that all the selected coumarins have great oral absorption and thus greater bioavailability. Moreover, all the drugs displayed good blood-brain barrier permeability values which is a necessary parameter to consider for developing

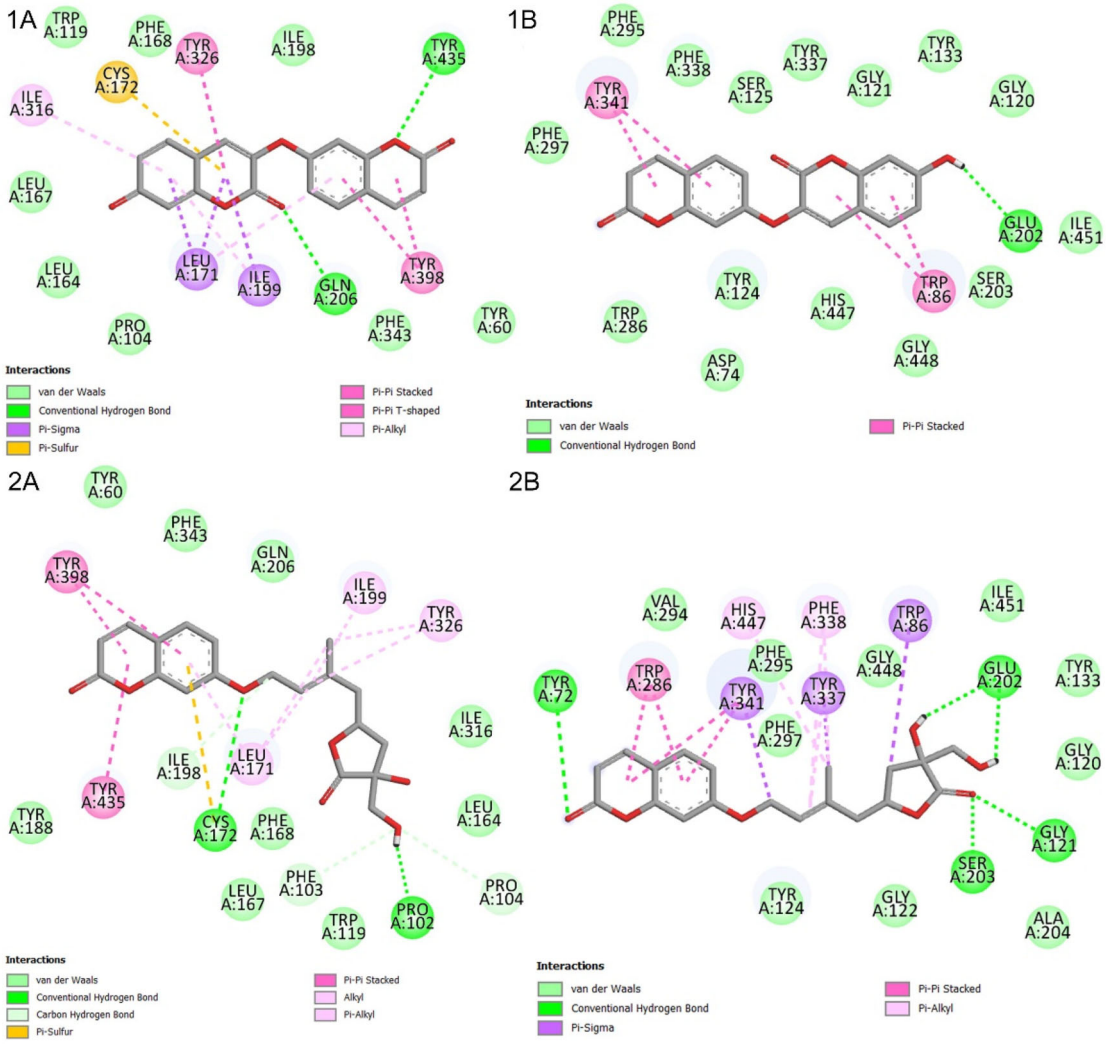

Figure 8. Protein-ligand interaction diagrams of the selected coumarin candidates. (1A) CDB0738-MAO-B complex; (2A) CDB0046-MAO-B complex; (1B) CDB0738-AChE complex; (2B) CDB0046-AChE complex.

Table 7. ADMET prediction results of the selected coumarins.

Compound	Water solubility	Intestinal absorption	BBB permeability	CNS permeability	CYP2D6 interaction	Ames toxicity	Liver toxicity
C18	−4.2	93.7	0.2	−2.1	Yes	Yes	Yes
E20	−4.6	93.7	0.2	−1.5	Yes	No	Yes
CDB0738	−5.5	99.4	−0.2	−1.7	No	No	No
CDB0046	−3.6	97.3	−0.5	−2.9	No	No	No
CDB0042	−3.9	96.7	−0.3	−2.4	No	Yes	No
CDB0885	−3.4	78.2	−0.9	−3.4	No	Yes	Yes
CDB0794	−3.3	94.2	−0.2	−2.2	No	Yes	No
CDB0029	−3.4	100	−0.5	−2.1	No	Yes	Yes
CDB0375	−4.3	92.5	−0.7	−2.9	No	No	Yes
CDB0062	−3.5	100	−0.8	−3.1	No	No	No
CDB0469	−3.4	100	−0.1	−2.9	No	Yes	No
CDB0821	−4.4	95.2	−0.6	−1.9	No	No	No

brain-acting drugs. CNS permeability is another parameter that takes the blood-brain permeability surface (logPS) as a factor. Most of the selected coumarins are considered to penetrate the CNS while some others have average permeability, CDB0885 and CDB0062 are considered unable to penetrate the CNS due to their low logPS valules (< -3.0). Furthermore, all compounds, excluding the reference ligands, were identified as non-inhibitors of CYP2D6, which is particularly necessary for drugs acting on the brain since the expression of CYP2D6 is higher in the brain and is involved in metabolizing endogenous neural compounds suggesting its neuroprotective properties. Ames toxicity revealed that six coumarins including the reference MAO-B inhibitor are predicted as mutagenic. Hepatotoxicity also predicted three coumarins in addition to the reference ligands as positive for inducing liver related injuries.

Water solubility: Solubility of the molecule in water at 25 °C (log mol/L); Intestinal absorption: Percentage that will be absorbed through the human intestine; BBB permeability: Logarithmic ratio of brain to plasma drug concentrations.

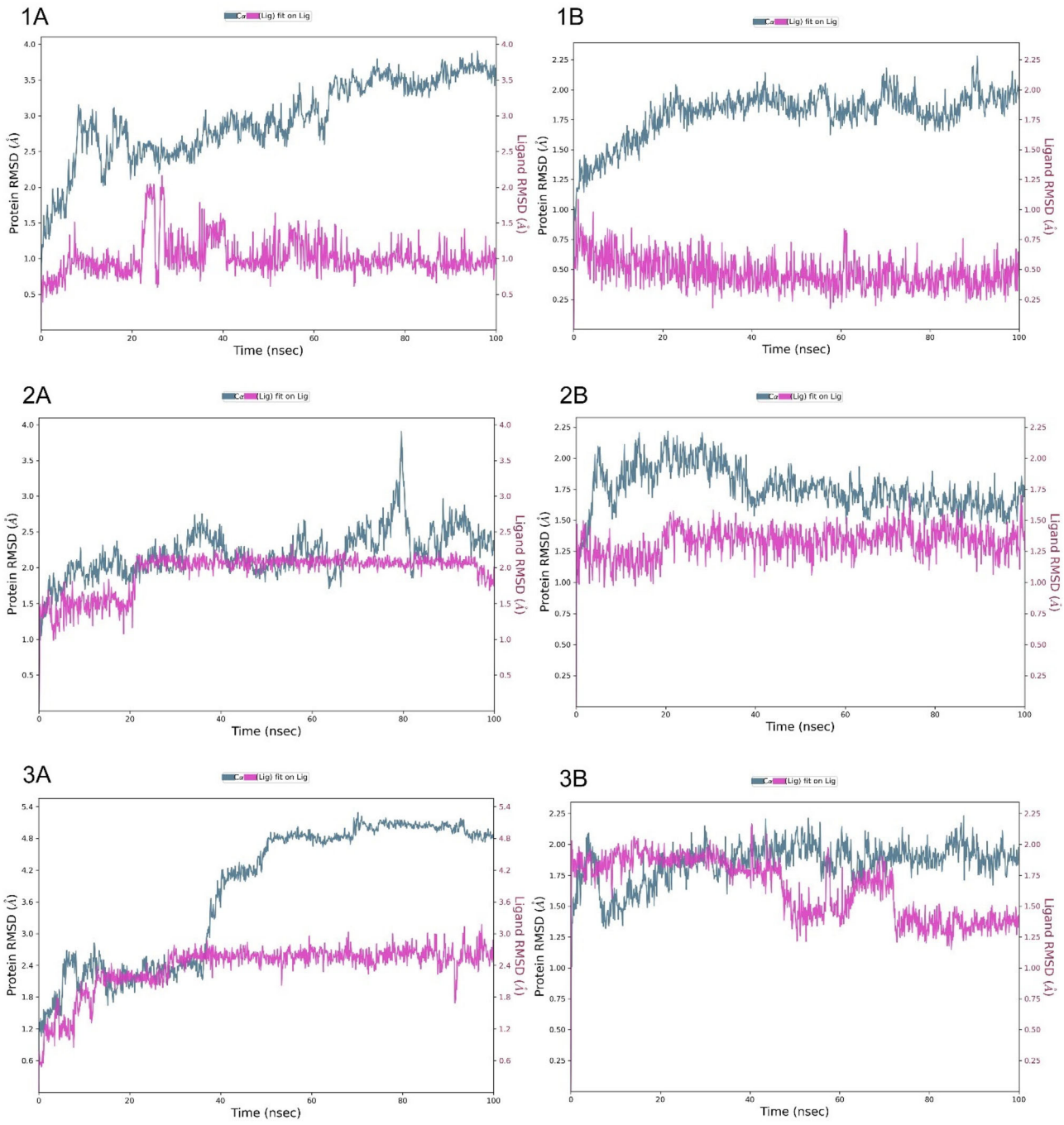

Figure 9. Time-dependent protein–ligand root-mean square deviation (RMSD) plots of MAO-B in complex with reference inhibitor (C18) (1A), CDB00738 (2A), CDB00046 (3A) and AChE in complex with reference inhibitor (donepezil) (1B), CDB00738 (2B), CDB00046 (3B).

(logBB $>$ 0.3 is considered to cross the BBB while molecules with logBB$<$-1 are poorly distributed to the brain; CNS permeability: Compounds with a logPS$>$-2 are considered to penetrate CNS, while those with logPS$<$-3 are considered as unable to penetrate the CNS; Ames toxicity: A positive prediction indicates that the compound is mutagenic and therefore may act as a carcinogen; Liver toxicity: Drug-induced liver injury.

3.5. Molecular dynamics simulations

The best coumarin candidates namely, CDB0738 and CDB0046 in complex with MAO-B and AChE were selected from the molecular docking study in addition to the reference protein-ligand complexes to perform molecular dynamics simulations and assess their stability over time. Various molecular dynamics analyses were conducted such as root-mean square deviation (RMSD), root-mean square fluctuation (RMSF), protein-ligand interactions and ligand properties variation with respect to the simulation period.

3.5.1. Root-mean square deviation

The RMSD plots of the selected coumarin candidates and the reference inhibitors in complex with MAO-B and AChE are shown in Figure 9. The RMSD values indicate how much the

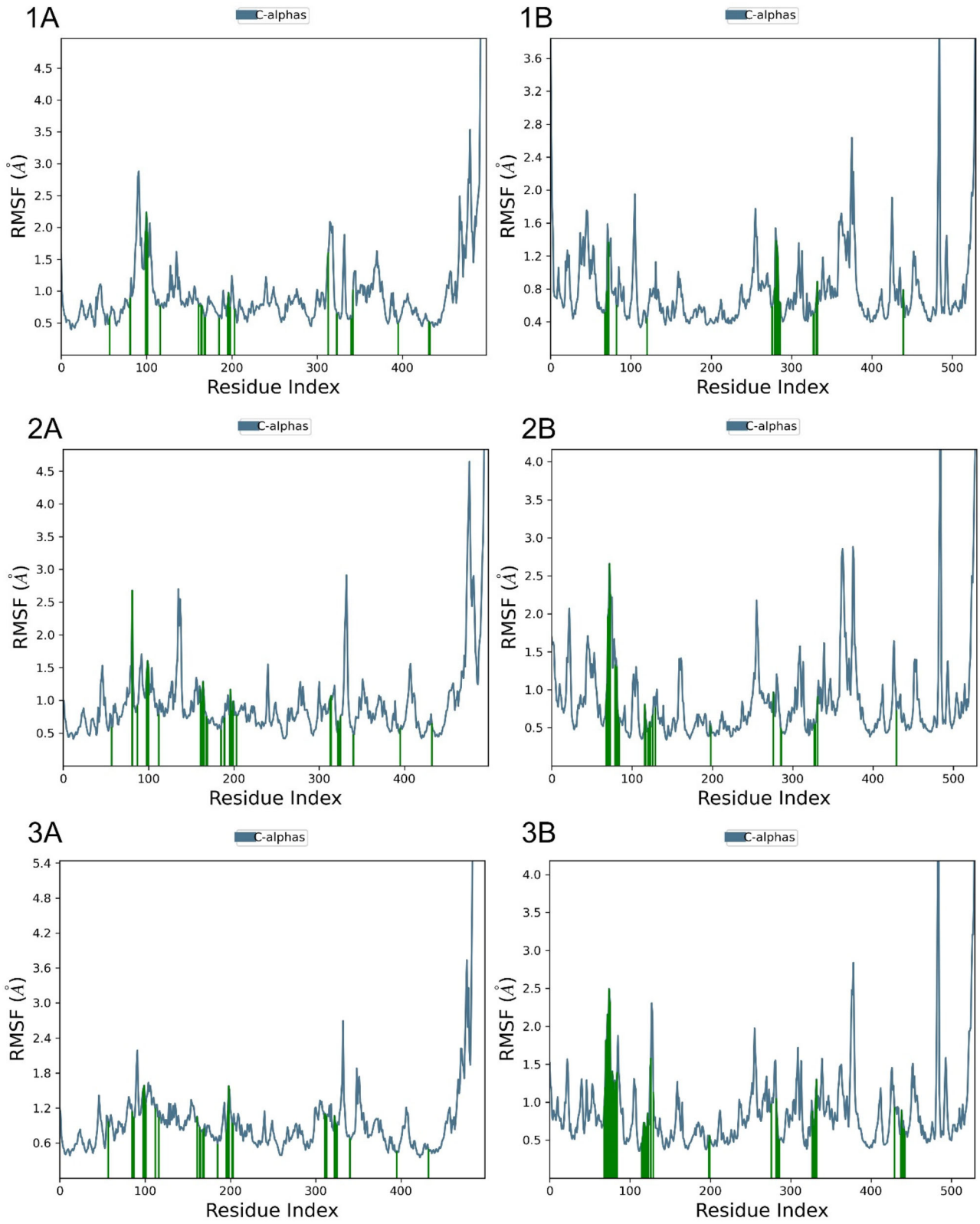

Figure 10. Time-dependent protein–ligand root-mean square fluctuation (RMSF) plots of MAO-B in complex with reference inhibitor (C18) (1A), CDB00738 (2A), CDB00046 (3A) and AChE in complex with reference inhibitor (donepezil) (1B), CDB00738 (2B), CDB00046 (3B).

protein and ligand have moved from their starting positions and how stable the complex is as a result.

The CDB0738-MAOB complex showed low RMSD values of around 2.5 Å, which is acceptable for protein-ligand complexes (Ahmad et al., 2022). This suggests that the complex is relatively stable and that the protein and ligand have only moved slightly from their initial positions. The CDB0046-MAOB complex, however, showed larger RMSD values of

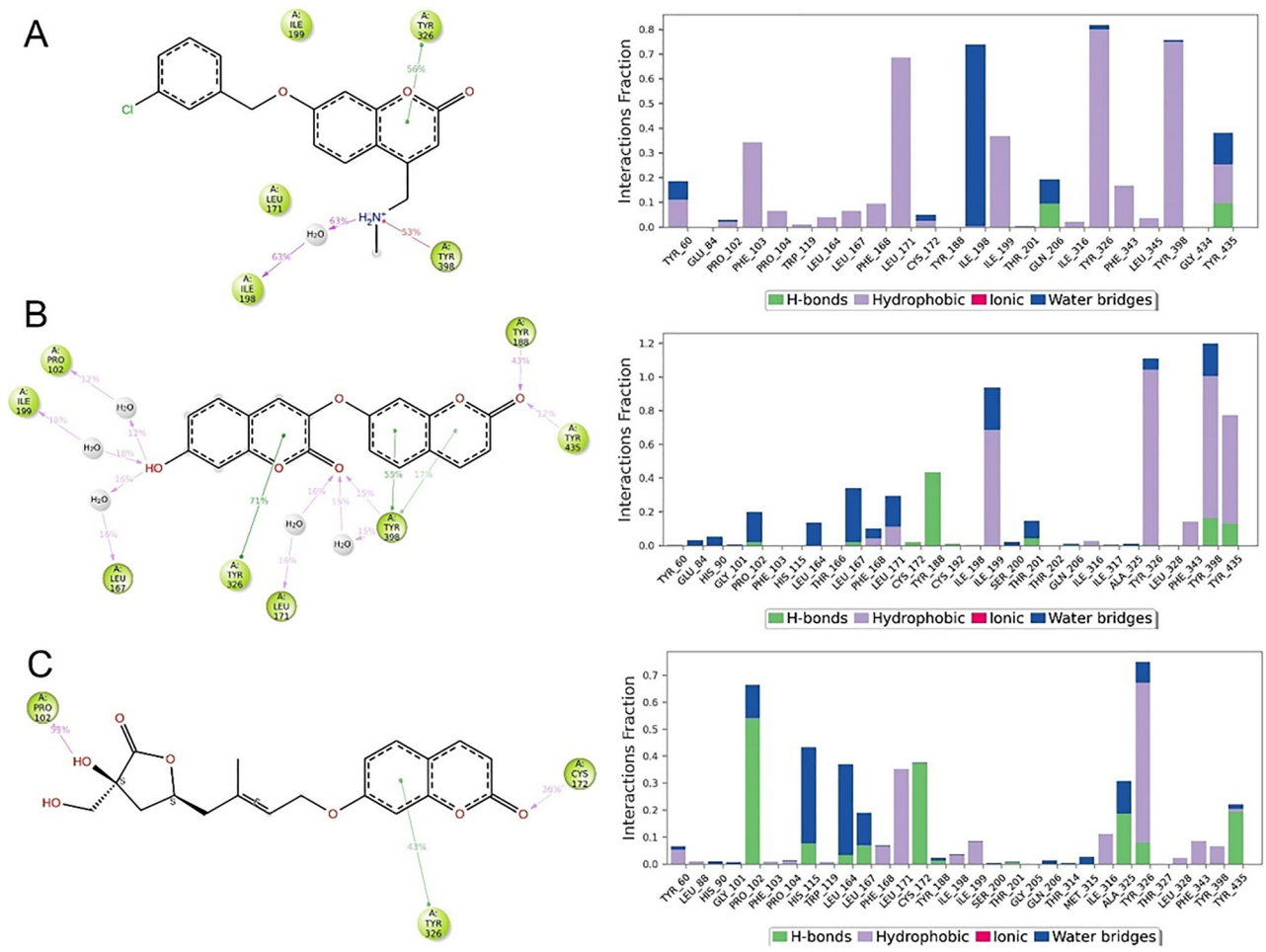

Figure 11. Simulation interaction diagrams and histograms of C18 (A), CDB0738 (B) and CDB0046 (C) in complex with MAO-B. Residues involved in the interactions are presented in the x axis, the y axis presents the normalized value of the temporal length of the interactions during the simulation.

around 4 Å, indicating that the complex is less stable and that the protein has moved significantly over time. This could be due to the bulky size of the CDB0046 molecule inducing structural changes to the protein. This is also noted in the ligand RMSD which revealed deviations around 1, 2, and 2.4 Å for the reference inhibitor, CDB0738 and CDB0046 respectively.

For the AChE complex, the reference complex displayed RMSD values of around 2 Å, which is also considered acceptable (Kua et al., 2002). The CDB0738-AChE complex exhibited even lower RMSD values of around 1.75 Å, indicating that the complex is more stable than the reference complex. The CDB0046-AChE complex showed similar RMSD values to the reference complex, around 2 Å. Regarding the ligand RMSD values, Donepezil showed very low values ranging between 0.25 and 0.75 Å with respect to the protein, indicating that it is highly stable in the protein cavity. CDB0738 showed slightly higher values of around 1.25 and 1.5 Å, while CDB0046 was the least stable with values around 2 Å during the first 75 ns but stabilized to around 1.25 and 1.5 Å for the rest of the simulation.

Overall, the RMSD results suggest that CDB0738 may be a more suitable candidate for inhibition of MAO-B and AChE than the reference inhibitors and CDB0046 due to its stability in the protein cavity.

3.5.2. Root-mean square fluctuation

The RMSF is a valuable tool in analyzing the fluctuations of individual atoms along the protein chain during molecular dynamics simulations (Martínez, 2015). The RMSF plots shown in Figure 10 display the fluctuations in the protein structure, with peaks indicating areas of the protein that show the highest amount of movement. It is common to see that the ends (N-terminal and C-terminal) of the protein fluctuate more than any other part of the protein structure. On the other hand, secondary structure elements like α-helices and β-strands tend to be more rigid and less flexible compared to loop regions, and thus, exhibit lower levels of fluctuation. In addition, protein residues that interact with the ligand are identified on the RMSF plot by green-colored vertical bars, highlighting the specific areas of the protein that are involved in binding with the ligand.

Figure 10 shows the residues of the MAO-B enzyme in complex with the selected coumarins remained stable throughout the simulation. The results indicate the highest fluctuations were at 5 Å for all three MAO-B complexes, but these fluctuating residues are not involved in ligand binding as they are in the C-terminal region, indicating slight conformational change.

For AChE, the RMSF analysis displays some high fluctuations around 3 Å, however, the ligand-binding regions are

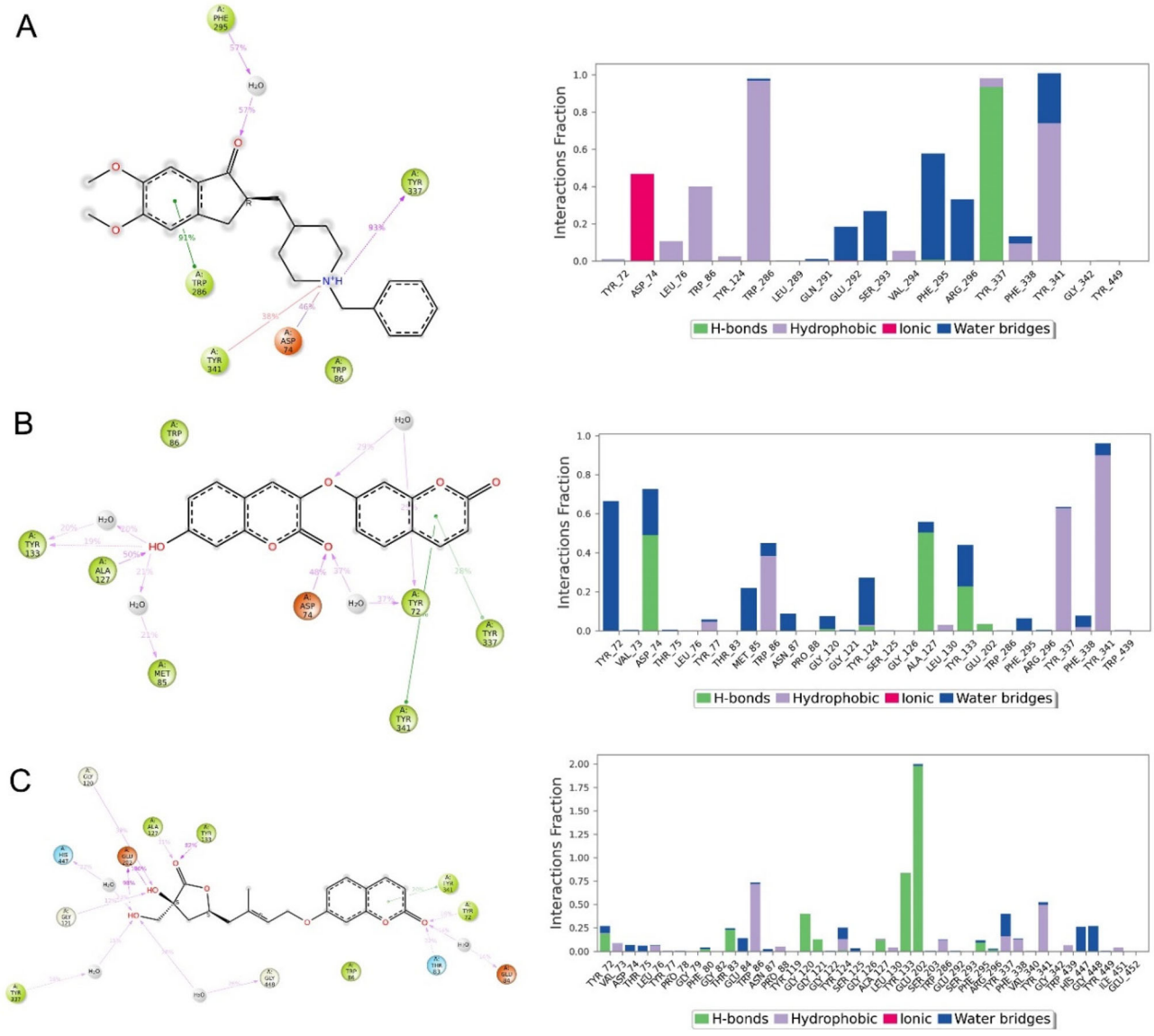

Figure 12. Simulation interaction diagrams and histograms of E20 (A), CDB0738 (B) and CDB0046 (C) in complex with AChE. Residues involved in the interactions are presented in the x axis, the y axis presents the normalized value of the temporal length of the interactions during the simulation.

less fluctuating, with values around 1.6 Å in the reference complex. The CDB0738-AChE structure shows high flexibility near residues 300–400, and similar fluctuations were observed in CDB0046-AChE and in the literature (Pitchai et al., 2020). For all complexes, the regions with the highest mobility were dispersed around C-terminal residues 480–520, considered typical as it is an unstructured part of the protein.

3.5.3. Protein-ligand interactions

The simulation results revealed the role of each amino acid in protein-ligand interactions. The diagrams of MAO-B complex interactions (Figure 11) showed that most of the interactions with the active site of MAO-B are hydrophobic. Additionally, two hydrogen bonds were preserved in the reference complex, involving Gln-206 and Tyr-435, which are common in MAO-B inhibitors (Azam et al., 2012). Another water-mediated hydrogen bond was observed involving Ile-198 in the 'gating' cavity. The hydrophobic nature of the cavity resulted in most of the other interactions being hydrophobic. The key hydrophobic interactions were mainly with Leu-171, Ile-199, Tyr-326, Tyr-398, and Tyr-435. Furthermore, CDB0738 formed hydrogen bonds with Tyr-188, Tyr-398, and Tyr-435 of the aromatic cage. The simulation also revealed the presence of strong water bridges involving Pro-102, Leu-171, and Ile-199. Finally, CDB0046 mainly interacted with Pro-102 of the entrance cavity and Cys-172 *via* hydrogen bonds, due to the molecule's length. Other hydrophobic interactions involving Leu-171 and Tyr-326 were also observed.

Figure 12 highlights the interactions between the binding pocket residues of AChE and docked ligands. The plot provides a comprehensive understanding of the preservation of essential interactions such as hydrogen bonding, hydrophobic interactions, and water-mediated contacts

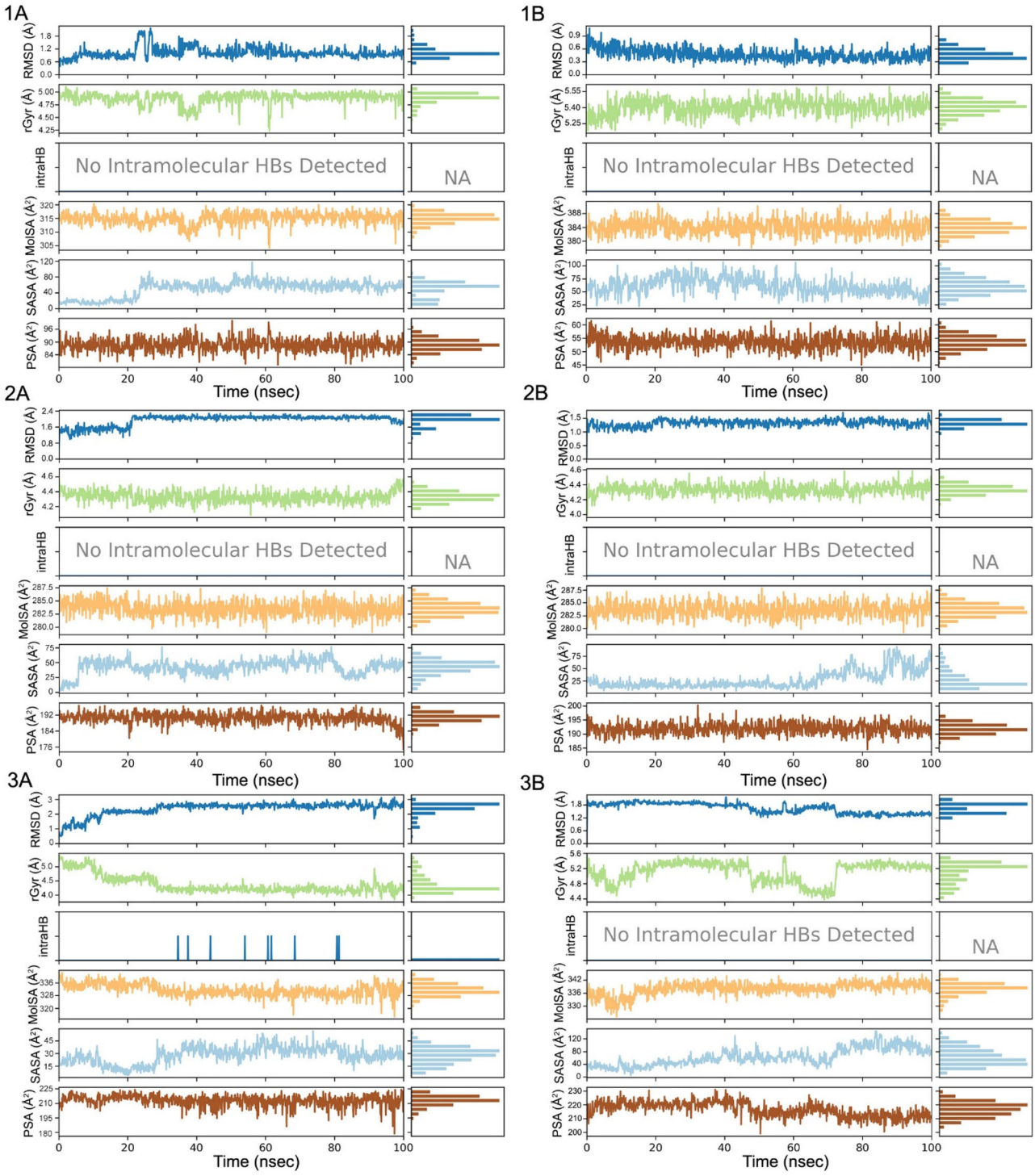

Figure 13. Variation in the ligand properties (RMSD, rGyr, intraHB, MolSA, SASA and PSA) with respect to the simulation time. (1A) The reference MAO-B inhibitor, C18; (2A) CDB0738; (3A) CDB0046; (1B) the reference AChE inhibitor, Donepezil; (2B) CDB0738; 3B) CDB0046.

throughout the simulation, as supported by several studies in the literature (Daoud et al., 2018; Shen et al., 2002). Donepezil, the reference inhibitor, has been shown to form a hydrogen bond with Tyr-337 in the PAS. This amino acid is known to bind the quaternary trimethylammonium tail group of acetylcholine and may therefore play a crucial role in inhibiting AChE activity (Messaad et al., 2022; Zhou et al., 2010). The ionic interaction with Asp-74 in the PAS has also been shown to play a role in the specificity of cationic organophosphonates as it acts as a proton acceptor (Barak et al., 1994; Sugimoto et al., 2000). The hydrophobic interactions with Trp-86, Trp-286, and Tyr-341 in both the CAS and PAS have been shown to stabilize the ligand in the binding pocket and contribute to the inhibition (Hosea et al., 1996).

For CDB0738, the three hydrogen bonds with Asp-74, Ala-127, and Tyr-133 in the PAS have been shown to play a critical role in inhibition (Dhananjayan et al., 2013). CDB0046 has important hydrogen bonds with Tyr-133 in the PAS and Glu-202 in the CAS, as well as hydrophobic interactions with Trp-86 and Tyr-341 in both anionic sites.

3.5.4. Ligand properties variation

To assess the stability of the selected compounds in the cavities of MAO-B and AChE, five molecular properties namely, ligand RMSD, radius of gyration (rGyr), molecular surface area (MolSA), solvent accessible surface area (SASA), and polar surface area (PSA) were analyzed over a 100 ns simulation period, as depicted in Figure 13. The ligand RMSD measures the deviation of a ligand's conformation relative to a reference conformation, usually the first frame (Krishnaveni, 2015). The RMSD values of all compounds remained below 2 Å throughout the simulation for AChE. As for MAO-B, CDB0738 showed fluctuations at 2.4 Å before stabilizing at 2 Å at the end of the simulation, meanwhile CDB0046 exhibited some deviations around 3 Å through all the simulation. The radius of gyration, which measures the 'extendedness' of a ligand and is equivalent to its principal moment of inertia, remained constant and ranged from 4 to 5 Å for the selected compounds which is due to the size of the ligands and their flexibility resulting in more mobility, thus reducing their compactness. The MolSA was calculated using a probe radius of 1.4 Å and represents the van der Waals surface area. The SASA area reflects the surface area accessible to water molecules, and the polar surface area represents the solvent-accessible surface area that is contributed by only oxygen and nitrogen atoms. Despite the exposure and rotational flexibility of the protein and the ligand, deviations in the surface area (MolSA, SASA and PSA) were found to be higher in CDB0046 when compared to CDB0738 indicating a higher degree of charged surface area in the former which can affect the solubility and stability of a molecule in polar solvents, such as water. For MolSA and SASA, the size of the molecule and the specific solvent used can affect the values obtained. For example, larger molecules will generally have larger MolSA and SASA values, while smaller molecules will have smaller values. Similarly, different solvents may lead to different MolSA and SASA values, depending on the size and properties of the solvent molecules (Ferdausi et al., 2022).

4. Conclusion

MAO-B and AChE are considered relevant targets when developing neuroprotective drugs against Parkinson's and Alzheimer's disease. Coumarins and their derivatives have been synthetized for decades and extensively evaluated against neurodegenerative diseases, however natural coumarins are yet to be investigated. The present study aimed to collect all available naturally occurring coumarins with their corresponding natural sources. A chemical library was designed to bioprospect novel coumarin candidates as neuroprotective agents. QSAR models were generated using all available MAO-B and AChE inhibitors with their reported experimental activity to screen for potential MAO-B and AChE inhibitors from natural coumarins. Our results revealed ten coumarins with pIC_{50} values > 6. The selected coumarins were subjected for molecular docking study to assess their binding affinities and molecular interactions. CDB0738 and CDB0046 showed potential as inhibitors for MAO-B and AChE. Both compounds showed promising interactions with critical amino acids involved in the stability and the specificity of MAO-B and AChE, indicating their potential affinity and selectivity towards these enzymes. Molecular dynamics were performed to analyze the stability of the protein-ligand complexes over 100 ns simulation period. Our results indicated that CDB0738 had the lowest RMSD values, around 2.5 Å for MAO-B and 1.75 Å for AChE, indicating that it was the most stable complex among the candidates. Moreover, RMSF analysis showed typical fluctuations in the N- and C-terminal residues, however the ligand-binding regions were less fluctuating. Analysis of molecular interactions revealed the presence of key hydrogen bonds and highlighted the importance of hydrophobic interactions as reported in the literature. For AChE, the two coumarin candidates, CDB0738 and CDB0046, formed critical interactions with residues from the CAS and the PAS in a similar manner to the reference inhibitor, Donepezil. Finally, the *in silico* ADMET parameters of the screened coumarins were found to be acceptable and within the suitable range for human use. This study provides renewed hope that naturally occurring products, especially coumarins could potentially lead to the development of a new neuroprotective drug for the treatment of Parkinson's and Alzheimer's disease. However, additional *in vitro* and *in vivo* studies are needed to confirm their effectiveness.

Acknowledgments

We would like to thank Francisco Javier Luque Garriga, Professor in the Department of Chemical Physics, University of Barcelona, Spain, for his assistance. His contribution is sincerely appreciated and gratefully acknowledged.

Disclosure statement

No potential conflict of interest was reported by the authors.

Funding

The authors gratefully acknowledge ProteinsInsights, Nangal Raya, New Delhi, India, for providing the computational resources essential for the successful completion of this research.

ORCID

Amal Maurady http://orcid.org/0000-0001-9298-717X

References

Ahmad, I., Kumar, D., & Patel, H. (2022). Computational investigation of phytochemicals from Withania somnifera (Indian ginseng/ashwagandha) as plausible inhibitors of GluN2B-containing NMDA receptors. *Journal of Biomolecular Structure & Dynamics*, *40*(17), 7991–8003. https://doi.org/10.1080/07391102.2021.1905553

Azam, F., Madi, A. M., & Ali, H. I. (2012). Molecular docking and prediction of pharmacokinetic properties of dual mechanism drugs that block MAO-B and adenosine A2A receptors for the treatment of Parkinson's disease. *Journal of Young Pharmacists: JYP*, *4*(3), 184–192. https://doi.org/10.4103/0975-1483.100027

Bara-Jimenez, W., Sherzai, A., Dimitrova, T., Favit, A., Bibbiani, F., Gillespie, M., Morris, M. J., Mouradian, M. M., & Chase, T. N. (2003).

Adenosine A2A receptor antagonist treatment of Parkinson's disease. *Neurology*, *61*(3), 293–296. https://doi.org/10.1212/01.wnl.0000073136.00548.d4

Barak, D., Kronman, C., Ordentlich, A., Ariel, N., Bromberg, A., Marcus, D., Lazar, A., Velan, B., & Shafferman, A. (1994). Acetylcholinesterase peripheral anionic site degeneracy conferred by amino acid arrays sharing a common core. *Journal of Biological Chemistry*, *269*(9), 6296–6305. https://doi.org/10.1016/S0021-9258(17)37371-4

Barnham, K. J., Masters, C. L., & Bush, A. I. (2004). Neurodegenerative diseases and oxidative stress. *Nature Reviews. Drug Discovery*, *3*(3), 205–214. https://doi.org/10.1038/nrd1330

Bibbiani, F. O. H. J. D., Oh, J. D., Petzer, J. P., Castagnoli, N., Jr, Chen, J. F., Schwarzschild, M. A., & Chase, T. N. (2003). A2A antagonist prevents dopamine agonist-induced motor complications in animal models of Parkinson's disease. *Experimental Neurology*, *184*(1), 285–294. https://doi.org/10.1016/s0014-4886(03)00250-4

Binda, C., Wang, J., Pisani, L., Caccia, C., Carotti, A., Salvati, P., Edmondson, D. E., & Mattevi, A. (2007). Structures of human monoamine oxidase B complexes with selective noncovalent inhibitors: Safinamide and coumarin analogs. *Journal of Medicinal Chemistry*, *50*(23), 5848–5852. https://doi.org/10.1021/jm070677y

Biovia, D. S. (2017). *Discovery studio visualizer*. 936.

Boulaamane, Y., Ahmad, I., Patel, H., Das, N., Britel, M. R., & Maurady, A. (2023). Structural exploration of selected C6 and C7-substituted coumarin isomers as selective MAO-B inhibitors. *Journal of Biomolecular Structure and Dynamics*, *41*(6), 2326–2340. https://doi.org/10.1080/07391102.2022.2033643

Boulaamane, Y., Ibrahim, M. A., Britel, M. R., & Maurady, A. (2022). In silico studies of natural product-like caffeine derivatives as potential MAO-B inhibitors/AA2AR antagonists for the treatment of Parkinson's disease. *Journal of Integrative Bioinformatics*, *19*(4), 16-17. https://doi.org/10.1515/jib-2021-0027

Bowers, K. J., Chow, E., Xu, H., Dror, R. O., Eastwood, M. P., Gregersen, B. A., … Shaw, D. E. (2006). *Scalable algorithms for molecular dynamics simulations on commodity clusters* [Paper presentation]. In Proceedings of the 2006 ACM/IEEE Conference on Supercomputing, November). (pp. 84–es). https://doi.org/10.1145/1188455.1188544

Brühlmann, C., Ooms, F., Carrupt, P. A., Testa, B., Catto, M., Leonetti, F., Altomare, C., & Carotti, A. (2001). Coumarins derivatives as dual inhibitors of acetylcholinesterase and monoamine oxidase. *Journal of Medicinal Chemistry*, *44*(19), 3195–3198. https://doi.org/10.1021/jm010894d

Burggraaff, L., van Vlijmen, H. W. T., IJzerman, A. P., & van Westen, G. J. P. (2020). Quantitative prediction of selectivity between the A1 and A2A adenosine receptors. *Journal of Cheminformatics*, *12*(1), 33. https://doi.org/10.1186/s13321-020-00438-3

Carradori, S., D'Ascenzio, M., Chimenti, P., Secci, D., & Bolasco, A. (2014). Selective MAO-B inhibitors: A lesson from natural products. *Molecular Diversity*, *18*(1), 219–243. https://doi.org/10.1007/s11030-013-9490-6

Chaudhuri, K. R., Healy, D. G., & Schapira, A. H, National Institute for Clinical Excellence. (2006). Non-motor symptoms of Parkinson's disease: Diagnosis and management. *The Lancet. Neurology*, *5*(3), 235–245. https://doi.org/10.1016/S1474-4422(06)70373-8

Chen, J. H., Huang, T. W., & Hong, C. T. (2021). Cholinesterase inhibitors for gait, balance, and fall in Parkinson disease: A meta-analysis. *Npj Parkinson's Disease*, *7*(1), 1–7. https://doi.org/10.1038/s41531-021-00251-1

Cheung, J., Rudolph, M. J., Burshteyn, F., Cassidy, M. S., Gary, E. N., Love, J., Franklin, M. C., & Height, J. J. (2012). Structures of human acetylcholinesterase in complex with pharmacologically important ligands. *Journal of Medicinal Chemistry*, *55*(22), 10282–10286. https://doi.org/10.1021/jm300871x

Daoud, I., Melkemi, N., Salah, T., & Ghalem, S. (2018). Combined QSAR, molecular docking and molecular dynamics study on new Acetylcholinesterase and Butyrylcholinesterase inhibitors. *Computational Biology and Chemistry*, *74*, 304–326. https://doi.org/10.1016/j.compbiolchem.2018.03.021

Dean, F. M. (1952). Naturally occurring coumarins. Fortschritte der Chemie Organischer Naturstoffe/Progress in the Chemistry of Organic Natural Products/Progrès Dans La Chimie Des Substances Organiques Naturelles, 225–291.

Dhananjayan, K., Sumathy, A., & Palanisamy, S. (2013). Molecular docking studies and in-vitro acetylcholinesterase inhibition by terpenoids and flavonoids. *Asian Journal of Research in Chemistry*, *6*(11), 1011–1017.

Di Paolo, M. L., Cozza, G., Milelli, A., Zonta, F., Sarno, S., Minniti, E., Ursini, F., Rosini, M., & Minarini, A. (2019). Benextramine and derivatives as novel human monoamine oxidases inhibitors: An integrated approach. *The FEBS Journal*, *286*(24), 4995–5015. https://doi.org/10.1111/febs.14994

Dias, V., Junn, E., & Mouradian, M. M. (2013). The role of oxidative stress in Parkinson's disease. *Journal of Parkinson's Disease*, *3*(4), 461–491. https://doi.org/10.3233/JPD-130230

Ding, Y., Chen, M., Guo, C., Zhang, P., & Wang, J. (2021). Molecular fingerprint-based machine learning assisted QSAR model development for prediction of ionic liquid properties. *Journal of Molecular Liquids*, *326*, 115212. https://doi.org/10.1016/j.molliq.2020.115212

Dugger, B. N., & Dickson, D. W. (2017). Pathology of neurodegenerative diseases. *Cold Spring Harbor Perspectives in Biology*, *9*(7), a028035. https://doi.org/10.1101/cshperspect.a028035

Edmondson, D. E., & Newton-Vinson, P. (2001). The covalent FAD of monoamine oxidase: Structural and functional role and mechanism of the flavinylation reaction. *Antioxidants & Redox Signaling*, *3*(5), 789–806. https://doi.org/10.1089/15230860152664984

Ekström, F., Gottinger, A., Forsgren, N., Catto, M., Iacovino, L. G., Pisani, L., & Binda, C. (2022). Dual Reversible Coumarin Inhibitors Mutually Bound to Monoamine Oxidase B and Acetylcholinesterase Crystal Structures. *ACS Medicinal Chemistry Letters*, *13*(3), 499–506. https://doi.org/10.1021/acsmedchemlett.2c00001

Ferdausi, N., Islam, S., Rimti, F. H., Quayum, S. T., Arshad, E. M., Ibnat, A., Islam, T., Arefin, A., Ema, T. I., Biswas, P., Dey, D., & Azad, S. A. (2022). Point-specific interactions of isovitexin with the neighboring amino acid residues of the hACE2 receptor as a targeted therapeutic agent in suppressing the SARS-CoV-2 influx mechanism. *Journal of Advanced Veterinary and Animal Research*, *9*(2), 230–240. https://doi.org/10.5455/javar.2022.i588

Fukunishi, Y., & Lintuluoto, M. (2010). Development of chemical compound libraries for in silico drug screening. *Current Computer-Aided Drug Design*, *6*(2), 90–102. https://doi.org/10.2174/157340910791202450

Garrard, A. (2014). Coumarins. In *Encyclopedia of Toxicology*. (pp. 1052–1054). Elsevier. https://doi.org/10.1016/B978-0-12-386454-3.00798-3

Gola, J., Obrezanova, O., Champness, E., & Segall, M. (2006). ADMET property prediction: The state of the art and current challenges. *QSAR & Combinatorial Science*, *25*(12), 1172–1180. https://doi.org/10.1002/qsar.200610093

Halgren, T. A. (1996). Merck molecular force field. I. Basis, form, scope, parameterization, and performance of MMFF94. *Journal of Computational Chemistry*, *17*(5-6), 490–519. https://doi.org/10.1002/(SICI)1096-987X(199604)17:5/6<490::AID-JCC1>3.0.CO;2-P

Hosea, N. A., Radić, Z., Tsigelny, I., Berman, H. A., Quinn, D. M., & Taylor, P. (1996). Aspartate 74 as a primary determinant in acetylcholinesterase governing specificity to cationic organophosphonates. *Biochemistry*, *35*(33), 10995–11004. https://doi.org/10.1021/bi9611220

Huey, R., & Morris, G. M. (2008). *Using AutoDock 4 with AutoDocktools: A tutorial*. The Scripps Research Institute. 8, 54–56.

Jo, S., Kim, T., Iyer, V. G., & Im, W. (2008). CHARMM-GUI: A web-based graphical user interface for CHARMM. *Journal of Computational Chemistry*, *29*(11), 1859–1865. https://doi.org/10.1002/jcc.20945

Kaakkola, S. (2010). Problems with the present inhibitors and a relevance of new and improved COMT inhibitors in Parkinson's disease. *International Review of Neurobiology*, *95*, 207–225.

Kalia, L. V., Kalia, S. K., & Lang, A. E. (2015). Disease-modifying strategies for Parkinson's disease. *Movement Disorders: Official Journal of the Movement Disorder Society*, *30*(11), 1442–1450. https://doi.org/10.1002/mds.26354

Katari, S. K., Natarajan, P., Swargam, S., Kanipakam, H., Pasala, C., & Umamaheswari, A. (2016). Inhibitor design against JNK1 through e-pharmacophore modeling docking and molecular dynamics

simulations. *Journal of Receptor and Signal Transduction Research*, *36*(6), 558–571. https://doi.org/10.3109/10799893.2016.1141955

Khanam, S., Subitsha, A. J., & Sabu, S. (2021). Plants as a promising source for the treatment of parkinson disease: A systematic review. *IP International Journal of Comprehensive and Advanced Pharmacology*, *5*(4), 158–166. https://doi.org/10.18231/j.ijcaap.2020.032

Kim, S., Chen, J., Cheng, T., Gindulyte, A., He, J., He, S., Li, Q., Shoemaker, B. A., Thiessen, P. A., Yu, B., Zaslavsky, L., Zhang, J., & Bolton, E. E. (2019). PubChem 2019 update: Improved access to chemical data. *Nucleic Acids Research*, *47*(D1), D1102–D1109. https://doi.org/10.1093/nar/gky1033

Krishnaveni, M. (2015). Docking, simulation studies of desulphosinigrin–cyclin dependent kinase 2, an anticancer drug target. *Int. J. Pharm. Sci. Rev. Res*, *30*(2), 115–118.

Kua, J., Zhang, Y., & McCammon, J. A. (2002). Studying enzyme binding specificity in acetylcholinesterase using a combined molecular dynamics and multiple docking approach. *Journal of the American Chemical Society*, *124*(28), 8260–8267. https://doi.org/10.1021/ja020429l

Lacy, A., & O'Kennedy, R. (2004). Studies on Coumarins and Coumarin-Related Compounds to Determine their Therapeutic Role in the Treatment of Cancer. *Current Pharmaceutical Design*, *10*(30), 3797–3811. https://doi.org/10.2174/1381612043382693

Landrum, G. (2013). RDKit: A software suite for cheminformatics, computational chemistry, and predictive modeling.

Lang, A. E., & Marras, C. (2014). Initiating dopaminergic treatment in Parkinson's disease. *Lancet (London, England)*, *384*(9949), 1164–1166. https://doi.org/10.1016/S0140-6736(14)60962-4

Lee, A., & Gilbert, R. M. (2016). Epidemiology of Parkinson disease. *Neurologic Clinics*, *34*(4), 955–965. https://doi.org/10.1016/j.ncl.2016.06.012

Lin, J., Sahakian, D. C., De Morais, S. M., Xu, J. J., Polzer, R. J., & Winter, S. M. (2003). The role of absorption, distribution, metabolism, excretion and toxicity in drug discovery. *Current Topics in Medicinal Chemistry*, *3*(10), 1125–1154. https://doi.org/10.2174/1568026033452096

Lu, J. J., Pan, W., Hu, Y. J., & Wang, Y. T. (2012). Multi-target drugs: The trend of drug research and development. *PLoS One*. *7*(6), e40262. https://doi.org/10.1371/journal.pone.0040262

Martínez, L. (2015). Automatic identification of mobile and rigid substructures in molecular dynamics simulations and fractional structural fluctuation analysis. *PLoS One*. *10*(3), e0119264. https://doi.org/10.1371/journal.pone.0119264

Mateev, E., Valkova, I., Angelov, B., Georgieva, M., & Zlatkov, A. (2022). Validation through re-docking, cross-docking and ligand enrichment in various well-resoluted MAO-B receptors. *International Journal of Pharmaceutical Sciences and Research*. *13*, 1099–1107.

McKinney, W. (2011). pandas: A foundational Python library for data analysis and statistics. *Python for High Performance and Scientific Computing*, *14*(9), 1–9.

Melchionna, S., Ciccotti, G., & Lee Holian, B. (1993). Hoover NPT dynamics for systems varying in shape and size. *Molecular Physics*, *78*(3), 533–544. https://doi.org/10.1080/00268979300100371

Mendez, D., Gaulton, A., Bento, A. P., Chambers, J., De Veij, M., Félix, E., Magariños, M. P., Mosquera, J. F., Mutowo, P., Nowotka, M., Gordillo-Marañón, M., Hunter, F., Junco, L., Mugumbate, G., Rodriguez-Lopez, M., Atkinson, F., Bosc, N., Radoux, C. J., Segura-Cabrera, A., Hersey, A., & Leach, A. R. (2019). ChEMBL: Towards direct deposition of bioassay data. *Nucleic Acids Research*, *47*(D1), D930–D940. https://doi.org/10.1093/nar/gky1075

Messaad, M., Dhouib, I., Abdelhedi, M., & Khemakhem, B. (2022). Synthesis, bioassay and molecular docking of novel pyrazole and pyrazolone derivatives as acetylcholinesterase inhibitors. *Journal of Molecular Structure*, *1263*, 133105. https://doi.org/10.1016/j.molstruc.2022.133105

Milczek, E. M., Binda, C., Rovida, S., Mattevi, A., & Edmondson, D. E. (2011). The 'gating'residues Ile199 and Tyr326 in human monoamine oxidase B function in substrate and inhibitor recognition. *The FEBS Journal*, *278*(24), 4860–4869. https://doi.org/10.1111/j.1742-4658.2011.08386.x

Möller, D., Óprzynski, J., Müller, A., & Fischer, J. (1992). Prediction of thermodynamic properties of fluid mixtures by molecular dynamics simulations: Methane-ethane. *Molecular Physics*, *75*(2), 363–378. https://doi.org/10.1080/00268979200100291

Murray, R. D. (2002). The naturally occurring coumarins. Fortschritte der Chemie organischer Naturstoffe/Progress in the Chemistry of Organic Natural Products, 1–619.

Ntie-Kang, F. (2013). An in silico evaluation of the ADMET profile of the StreptomeDB database. *Springerplus*, *2*(1), 1–11. https://doi.org/10.1186/2193-1801-2-353

O'Boyle, N. M., Banck, M., James, C. A., Morley, C., Vandermeersch, T., & Hutchison, G. R. (2011). Open Babel: An open chemical toolbox. *Journal of Cheminformatics*, *3*(1), 1–14. https://doi.org/10.1186/1758-2946-3-33

Pasrija, P., Jha, P., Upadhyaya, P., Khan, M., & Chopra, M. (2022). Machine Learning and Artificial Intelligence: A Paradigm Shift in Big Data-Driven Drug Design and Discovery. *Current Topics in Medicinal Chemistry*, *22*(20), 1692–1727. https://doi.org/10.2174/1568026622666220701091339

Pires, D. E., Blundell, T. L., & Ascher, D. B. (2015). pkCSM: Predicting small-molecule pharmacokinetic and toxicity properties using graph-based signatures. *Journal of Medicinal Chemistry*, *58*(9), 4066–4072. https://doi.org/10.1021/acs.jmedchem.5b00104

Pitchai, A., Rajaretinam, R. K., Mani, R., & Nagarajan, N. (2020). Molecular interaction of human acetylcholinesterase with trans-tephrostachin and derivatives for Alzheimer's disease. *Heliyon*, *6*(9), e04930. https://doi.org/10.1016/j.heliyon.2020.e04930

Poewe, W., & Mahlknecht, P. (2020). Pharmacologic treatment of motor symptoms associated with Parkinson disease. *Neurologic Clinics*, *38*(2), 255–267. https://doi.org/10.1016/j.ncl.2019.12.002

Poewe, W., Seppi, K., Tanner, C. M., Halliday, G. M., Brundin, P., Volkmann, J., Schrag, A.-E., & Lang, A. E. (2017). Parkinson disease. *Nature Reviews Disease Primers*, *3*(1), 1–21. https://doi.org/10.1038/nrdp.2017.13

Pourshojaei, Y., Abiri, A., Eskandari, K., Haghighijoo, Z., Edraki, N., & Asadipour, A. (2019). phenoxyethyl piperidine/Morpholine Derivatives as pAS and cAS inhibitors of cholinesterases: Insights for future Drug Design. *Scientific Reports*, *9*(1), 1–19. https://doi.org/10.1038/s41598-019-56463-2

Radic, Z., Pickering, N. A., Vellom, D. C., Camp, S., & Taylor, P. (1993). Three distinct domains in the cholinesterase molecule confer selectivity for acetyl-and butyrylcholinesterase inhibitors. *Biochemistry*, *32*(45), 12074–12084. https://doi.org/10.1021/bi00096a018

Ranjan, A., Kumar, A., Gulati, K., Thakur, S., & Jindal, T. (2015). Role of aromatic amino acids in stabilizing organophosphate and human acetylcholinesterase complex. *Journal of Current Pharma Research*, *5*(4), 1632–1639. https://doi.org/10.33786/JCPR.2015.v05i04.006

Sander, T., Freyss, J., von Korff, M., & Rufener, C. (2015). DataWarrior: An open-source program for chemistry aware data visualization and analysis. *Journal of Chemical Information and Modeling*, *55*(2), 460–473. https://doi.org/10.1021/ci500588j

Sarker, S. D., & Nahar, L. (2017). Progress in the chemistry of naturally occurring coumarins. *Progress in the Chemistry of Organic Natural Products*, *106*, 241–304. https://doi.org/10.1007/978-3-319-59542-9_3

Shen, T., Tai, K., Henchman, R. H., & McCammon, J. A. (2002). Molecular dynamics of acetylcholinesterase. *Accounts of Chemical Research*, *35*(6), 332–340. https://doi.org/10.1021/ar010025i

Shivakumar, D., Williams, J., Wu, Y., Damm, W., Shelley, J., & Sherman, W. (2010). Prediction of absolute solvation free energies using molecular dynamics free energy perturbation and the OPLS force field. *Journal of Chemical Theory and Computation*, *6*(5), 1509–1519. https://doi.org/10.1021/ct900587b

Singla, R. K., Agarwal, T., He, X., & Shen, B. (2021). Herbal resources to combat a progressive & degenerative nervous system disorder-Parkinson's disease. *Current Drug Targets*, *22*(6), 609–630. https://doi.org/10.2174/1389450121999201013155202

Singla, D., Sharma, A., Kaur, J., Panwar, B., & Raghava, G. P. (2010). BIAdb: A curated database of benzylisoquinoline alkaloids. *BMC Pharmacology*, *10*(1), 8. https://doi.org/10.1186/1471-2210-10-4

Soine, T. O. (1964). Naturally occurring coumarins and related physiological activities. *Journal of Pharmaceutical Sciences*, *53*(3), 231–264. https://doi.org/10.1002/jps.2600530302

Stefanachi, A., Leonetti, F., Pisani, L., Catto, M., & Carotti, A. (2018). Coumarin: A natural, privileged and versatile scaffold for bioactive compounds. *Molecules*, *23*(2), 250. https://doi.org/10.3390/molecules23020250

Sugimoto, H., Yamanish, Y., Iimura, Y., & Kawakami, Y. (2000). Donepezil hydrochloride (E2020) and other acetylcholinesterase inhibitors. *Current Medicinal Chemistry*, *7*(3), 303–339. https://doi.org/10.2174/0929867003375191

Tarasova, O. A., Urusova, A. F., Filimonov, D. A., Nicklaus, M. C., Zakharov, A. V., & Poroikov, V. V. (2015). QSAR modeling using large-scale databases: Case study for HIV-1 reverse transcriptase inhibitors. *Journal of Chemical Information and Modeling*, *55*(7), 1388–1399. https://doi.org/10.1021/acs.jcim.5b00019

Tetko, I. V., & Engkvist, O. (2020). From big data to artificial intelligence: Chemoinformatics meets new challenges. *Journal of Cheminformatics*, *12*(1), 3. https://doi.org/10.1186/s13321-020-00475-y

Trott, O., & Olson, A. J. (2010). AutoDock Vina: Improving the speed and accuracy of docking with a new scoring function, efficient optimization, and multithreading. *Journal of Computational Chemistry*, *31*(2), 455–461. https://doi.org/10.1002/jcc.21334

Van Laar, T., De Deyn, P. P., Aarsland, D., Barone, P., & Galvin, J. E. (2011). Effects of cholinesterase inhibitors in Parkinson's disease dementia: A review of clinical data. *CNS Neuroscience & Therapeutics*, *17*(5), 428–441. https://doi.org/10.1111/j.1755-5949.2010.00166.x

Venugopala, K. N., Rashmi, V., & Odhav, B. (2013). Review on Natural Coumarin Lead Compounds for Their Pharmacological Activity. *BioMed Research International*, *2013*, 963248. https://doi.org/10.1155/2013/963248

Wang, J., Lai, S., Kong, Y., Yao, W., Chen, X., & Liu, J. (2022). The protonation state of Glu202 in acetylcholinesterase. *Proteins: Structure, Function, and Bioinformatics*, *90*(2), 485–492. https://doi.org/10.1002/prot.26243

Wu, Z., Zhu, M., Kang, Y., Leung, E. L.-H., Lei, T., Shen, C., Jiang, D., Wang, Z., Cao, D., & Hou, T. (2021). Do we need different machine learning algorithms for QSAR modeling? A comprehensive assessment of 16 machine learning algorithms on 14 QSAR data sets. *Briefings in Bioinformatics*, *22*(4), bbaa321. https://doi.org/10.1093/bib/bbaa321

Xia, R., & Mao, Z. H. (2012). Progression of motor symptoms in Parkinson's disease. *Neuroscience Bulletin*, *28*(1), 39–48. https://doi.org/10.1007/s12264-012-1050-z

Yusufzai, S. K., Khan, M. S., Sulaiman, O., Osman, H., & Lamjin, D. N. (2018). Molecular docking studies of coumarin hybrids as potential acetylcholinesterase, butyrylcholinesterase, monoamine oxidase A/B and β-amyloid inhibitors for Alzheimer's disease. *Chemistry Central Journal*, *12*(1), 1–57. https://doi.org/10.1186/s13065-018-0497-z

Zhao, L., Ciallella, H. L., Aleksunes, L. M., & Zhu, H. (2020). Advancing computer-aided drug discovery (CADD) by big data and data-driven machine learning modeling. *Drug Discovery Today*. *25*(9), 1624–1638. https://doi.org/10.1016/j.drudis.2020.07.005

Zhou, Y., Wang, S., & Zhang, Y. (2010). Catalytic reaction mechanism of acetylcholinesterase determined by Born − Oppenheimer ab initio QM/MM molecular dynamics simulations. *The Journal of Physical Chemistry. B*, *114*(26), 8817–8825. https://doi.org/10.1021/jp104258d